Cellular/Molecular

Genetic Demonstration of a Role for Stathmin in Adult Hippocampal Neurogenesis, Spinogenesis, and NMDA Receptor-Dependent Memory

Guillaume Martel,[1,2]* Shusaku Uchida,[1,3,4]* Charles Hevi,[1] Itzamarie Chévere-Torres,[1] Ileana Fuentes,[1] Young Jin Park,[1] Hannah Hafeez,[1] Hirotaka Yamagata,[3] Yoshifumi Watanabe,[3] and Gleb P. Shumyatsky[1]

[1]Department of Genetics, Rutgers, State University of New Jersey, Piscataway, New Jersey 08854, [2]Centre de Psychiatrie et Neurosciences, Inserm U894, 75014 Paris, France, [3]Division of Neuropsychiatry, Department of Neuroscience, Yamaguchi University Graduate School of Medicine, Yamaguchi 755-8505, Japan, and [4]Core Research for Evolutional Science and Technology, Japan Science and Technology Agency, Saitama 332-0012, Japan

Neurogenesis and memory formation are essential features of the dentate gyrus (DG) area of the hippocampus, but to what extent the mechanisms responsible for both processes overlap remains poorly understood. Stathmin protein, whose tubulin-binding and microtubule-destabilizing activity is negatively regulated by its phosphorylation, is prominently expressed in the DG. We show here that stathmin is involved in neurogenesis, spinogenesis, and memory formation in the DG. *tTA/tetO*-regulated bitransgenic mice, expressing the unphosphorylatable constitutively active *Stathmin4A* mutant (*Stat4A*), exhibit impaired adult hippocampal neurogenesis and reduced spine density in the DG granule neurons. Although *Stat4A* mice display deficient NMDA receptor-dependent memory in contextual discrimination learning, which is dependent on hippocampal neurogenesis, their NMDA receptor-independent memory is normal. Confirming NMDA receptor involvement in the memory deficits, *Stat4A* mutant mice have a decrease in the level of synaptic NMDA receptors and a reduction in learning-dependent CREB-mediated gene transcription. The deficits in neurogenesis, spinogenesis, and memory in *Stat4A* mice are not present in mice in which *tTA/tetO*-dependent transgene transcription is blocked by doxycycline through their life. The memory deficits are also rescued within 3 d by intrahippocampal infusion of doxycycline, further indicating a role for stathmin expressed in the DG in contextual memory. Our findings therefore point to stathmin and microtubules as a mechanistic link between neurogenesis, spinogenesis, and NMDA receptor-dependent memory formation in the DG.

Key words: dentate gyrus; fear; hippocampus; memory; microtubules; stathmin

Significance Statement

In the present study, we aimed to clarify the role of stathmin in neuronal and behavioral functions. We characterized the neurogenic, behavioral, and molecular consequences of the gain-of-function stathmin mutation using a bitransgenic mouse expressing a constitutively active form of stathmin. We found that stathmin plays an important role in adult hippocampal neurogenesis and spinogenesis. In addition, stathmin mutation led to impaired NMDA receptor-dependent and neurogenesis-associated memory and did not affect NMDA receptor-independent memory. Moreover, biochemical analysis suggested that stathmin regulates the synaptic transport of NMDA receptors, which in turn influence CREB-mediated gene transcription machinery. Overall, these data suggest that stathmin is an important molecule for neurogenesis, spinogenesis, and NMDA receptor-dependent learning and memory.

Introduction

Although the essential contribution of hippocampal formation to memory is well documented, the specific functions of its different subregions remain unclear. With recent evidence suggesting an important role of the dentate gyrus (DG) in learning and memory, the signaling pathways governing its function have started to

Received Nov. 3, 2014; revised Nov. 12, 2015; accepted Dec. 10, 2015.

Author contributions: G.M., S.U., and G.P.S. designed research; G.M., S.U., C.H., I.C.-T., I.F., Y.J.P., H.H., H.Y., and Y.W. performed research; G.M., S.U., C.H., Y.J.P., and H.H. analyzed data; G.M., S.U., and G.P.S. wrote the paper.

This work was supported by National Science Foundation, National Institutes of Health Grant R01 MH080328, Whitehall Foundation 2008-12-104, March of Dimes, and New Jersey Commission on Brain Injury Research, all to G.P.S., and in part by Grants-in-Aid from Japan Society for the Promotion of Science to S.U. and Y.W., Core Research for Evolutional Science and Technology, Japan Science and Technology Agency to S.U., and the Integrated Research on Neuropsychiatric Disorders performed under the Strategic Research Program for Brain Sciences from the MEXT of Japan to H.Y. The research was funded in part by the New Jersey Governor's Council for Medical Research and Treatment of Autism, Special Child Health and Early Intervention Services, New Jersey Department of Health and

emerge (Deng et al., 2010; Drew et al., 2013). Importantly, these pathways include neurotransmitter receptors, such as NMDA receptors (NMDARs) and their associated cell signaling network, which is critical for neurogenesis, synaptic plasticity, and memory formation (Tsien et al., 1996; Tang et al., 1999; Rampon et al., 2000; Nacher and McEwen, 2006; Tashiro et al., 2006; Hamilton et al., 2012; Drew et al., 2013). Activation of postsynaptic NMDARs triggers complex downstream signaling events, including cAMP response-element binding protein (CREB)-dependent gene transcription, which is critical for memory in many species (Bourtchuladze et al., 1994; Impey et al., 1996; Silva et al., 1998). To exert their physiological roles, NMDARs must be transported into dendrites and synaptic sites. Thus, the dendritic transport of NMDARs along microtubules is a prerequisite for NMDAR activity (Lau and Zukin, 2007; Yin et al., 2011). However, little is known about the mechanisms underlying the microtubule-based dendritic transport of NMDARs.

Microtubules have been implicated in neurogenesis, synaptic plasticity, and memory formation (Shumyatsky et al., 2005; Jaglin and Chelly, 2009; Jaworski et al., 2009; Hirokawa et al., 2010; Kapitein et al., 2010; Yin et al., 2011; Fuster-Matanzo et al., 2012; Uchida et al., 2014; Uchida and Shumyatsky, 2015). A major role of microtubules in neurons is to regulate the transport of proteins, mRNAs, and membrane organelles (Hirokawa et al., 2010). Among the microtubule-associated proteins, stathmin, a negative regulator of microtubule formation (Belmont and Mitchison, 1996), is highly but selectively expressed in certain regions of the adult mammalian brain, including the DG of the hippocampus, amygdala, and cortex (Amat et al., 1991; Shumyatsky et al., 2005). Stathmin is phosphorylated by various protein kinases (Beretta et al., 1993; Marklund et al., 1994; le Gouvello et al., 1998), which reduce its binding affinity for tubulin heterodimers (Di Paolo et al., 1997; Larsson et al., 1997), leading to stable microtubules and reduced microtubule dynamics. Overexpression in the DG of the *Stathmin4A* (*Stat4A*) mutant, which lacks four Ser residue phosphorylation sites and acts as a constitutively active form of stathmin, leads to deficits in microtubule dynamics, synaptic plasticity, and hippocampus-dependent memory (Uchida et al., 2014; Uchida and Shumyatsky, 2015).

In this study, we examined the role of stathmin in neurogenesis, dendritic development, and NMDAR-dependent memory formation. We found that stathmin is expressed in both immature and mature neurons in the DG. Using *Stat4A* mutant mice, we uncovered that stathmin activity is associated with adult hippocampal neurogenesis, spinogenesis, and NMDAR-dependent memory. Furthermore, stathmin activation reduced dendritic transport of the GluN2A and GluN2B subunits of NMDAR, learning-induced CREB phosphorylation, and immediate early gene expression. Therefore, this study demonstrates a novel role for stathmin in regulating the transport of NMDARs, which is required for neurogenesis, spinogenesis, and CREB-mediated gene transcription, as well as contextual memory.

Senior Services to G.P.S., S.U. was supported by the Japan Society for the Promotion of Science Postdoctoral Fellowships for Research Abroad. We thank Mark Mayford for providing the *tetO-LacZ* mouse line; and Dr. Noriko Kane-Goldsmith for technical advice.

The authors declare no competing financial interests.

*G.M. and S.U. contributed equally to this work.

Correspondence should be addressed to Dr. Gleb P. Shumyatsky, Department of Genetics, Rutgers, State University of New Jersey, Piscataway, NJ 08854. E-mail: gleb@biology.rutgers.edu.

DOI:10.1523/JNEUROSCI.4541-14.2016

 0270-6474/16/361186-18$15.00/0

Materials and Methods

Animals. Generation of the *GRP-tTA* knock-in and the *tetO-Stat4A:GFP* transgenic mice was previously described (Uchida et al., 2014). Experimental mice (wild-type [WT], *Stat4A* double mutant, *GRP-tTA,* and *tetO-Stat4A:GFP* mice) were generated by crossing the *GRP-tTA* with *tetO-Stat4A:GFP* mice. The *GRP-tTA x tetO-LacZ* double mutant mouse (see Fig. 2*B*) was generated by crossing the single mutant lines. The *tetO-LacZ* single mutant mouse was a gift from Mark Mayford. All mice were maintained on a 12 h light/dark cycle. Mice were 1–6 months old at the time of the experiments. This study was performed in strict accordance with the recommendations in the Guide for the Care and Use of Laboratory Animals of the National Institutes of Health. The Rutgers University Institutional Animal Care and Use Committee approved the protocol.

Immunohistochemistry. Immunohistochemistry was performed as previously described (Uchida et al., 2011b). Mice were deeply anesthetized with Avertin (250 mg/kg i.p.) and transcardially perfused with 4% PFA. Their brains were postfixed overnight in 4% PFA and cryoprotected in 30% sucrose. The brains were sectioned (30 μm) using a cryostat, and single or double immunofluorescence was performed on free-floating sections. Primary antibodies included the mouse monoclonal antibodies NeuN (1:1000, Millipore) and glial fibrillary acidic protein (GFAP) (1:500, Millipore), a rat polyclonal antibody against BrdU (1:500, Abcam), rabbit polyclonal antibodies against green fluorescent protein (GFP) (1:500, Invitrogen), stathmin (1:1000, Millipore), and goat rabbit polyclonal antibody against doublecortin (DCX) (1:500, Santa Cruz Biotechnology). Secondary antibodies were conjugated with AlexaFluor-488 or -568 (1:500, Invitrogen) or Cy3 (Jackson ImmunoResearch Laboratories). Images were acquired using an LSM 510 META laser confocal microscope (Zeiss) with multichannel excitation and detection options, including optimal factory-recommended filter configurations to minimize spectral bleed-through. To analyze cell proliferation, the number of BrdU-positive cells throughout the subgranular zone in every sixth bilateral section was counted. To analyze cell survival, the number of BrdU-positive cells throughout the granule cell layer in every sixth bilateral section was counted. The number of BrdU-positive cells was then multiplied by 6 to estimate the total number of BrdU-positive cells. To correct for overestimations linked to counting the same nucleus on 2 adjacent sections, the following formula was applied: $N = (n \times t)/(t + d)$, where t is the section thickness, d is the nuclear diameter, and n is the number of counted nuclei. To analyze cell type markers, BrdU-positive cells in the granule cell layer of each mouse were examined by confocal microscopy (LSM 510 META; Zeiss). Densitometric analyses of GFP expression was performed by measuring mean pixel intensity with the software ImageProPlus 7 (Media Cybernetics). DAB staining was performed as previously reported (Wang et al., 2008; David et al., 2009). A goat polyclonal antibody against DCX (1:500) was obtained from Santa Cruz Biotechnology. The secondary antibody was biotinylated donkey anti-goat IgG (1:500, Jackson ImmunoResearch Laboratories). Sections were developed using avidin-biotin complex (Vector Laboratories) and DAB kit. Bright-field images were taken with a bright-field microscope (Nikon). DCX^+ cells were subcategorized according to their dendritic morphology: DCX^+ cells with no tertiary dendritic processes and DCX^+ cells with complex, tertiary dendrites. The maturation index was defined as the ratio of DCX^+ cells possessing tertiary dendrites over the total DCX^+ cells.

BrdU labeling. BrdU (Sigma, 100 mg/kg, 10 ml/kg, i.p.) was administered to the mice as described previously (Uchida et al., 2011b). To analyze cell proliferation, 8- to 12-week-old mice were killed 2 h after a single injection of BrdU. To analyze cell survival and cell type, 8- to 12-week-old mice were given four injections of BrdU (once daily, 4 consecutive days) and killed after 4 weeks.

Analysis of dendritic length and spine density. Golgi staining was performed using the FD Rapid Golgi Stain kit according to the manufacturer's protocol (FD NeuroTechnologies) as previously reported (Uchida et al., 2011b). The brains were sliced using a Vibratome at a thickness of 100 μm. Bright-field microscopic (Nikon) images (at ×20 or ×60 magnification) of granule neurons in the DG neurons (80 neurons per genotype) and of principal neurons in the lateral amygdala neurons (40 neurons per genotype) were obtained.

Only fully impregnated neurons displaying dendritic trees without obvious truncations and isolated from neighboring impregnated neurons were retained for analysis. The total dendrite length was quantified by tracing entire granule neurons. Quantification of spine density was limited to dendrites 100–150 μm from the soma. Spine density is expressed as the number of spines per μm of dendritic length.

Drug infusion. Stereotaxic surgery and drug infusion were performed as previously reported (Uchida et al., 2014). Mice were implanted under general anesthesia (Avertin, 300 mg/kg i.p.) with two guide cannulae (0.4 mm diameter, 8 mm long) aimed vertically toward the dorsal hippocampus or the basolateral amygdala. Guide cannulae were implanted into hippocampus (−2.0 mm anteroposterior, ±1.3 mm mediolateral, −0.9 mm dorsoventral) or into the amygdala (−1.7 mm anteroposterior, ±3.25 mm mediolateral, −3.5 mm dorsoventral) (Paxinos and Franklin, 2001). Following surgery, the mice remained in the animal room for a recovery period of 10 d before the experimental phase began. At the end of the experiments, mice were killed and brain sections were used for checking the placement of guide cannulae.

Doxycycline (dox) administration. Food pellet containing dox (40 mg/kg) was obtained from Bio-Serv. For direct infusion of dox into the brain, bilateral intrahippocampal (0.3 μl/side) or intra-amygdala (0.2 μl/side) injections of dox (Sigma, 10 μg/ml in PBS) or PBS were performed on freely moving mice via injection cannulae (0.2 mm diameter, 0.9 mm long) attached to 5 μl Hamilton syringes via polyethylene catheter tubing. The syringes were held in a constant-rate infusion pump, and bilateral injections were conducted over a 3 min period. In all cases, correct injection flow rates were visually controlled. The cannulae were left in place for an additional 2 min before removal. Mice were injected once a day during 3 consecutive days with dox or PBS. The first injection occurred the day before the acquisition of one pairing fear conditioning protocol; the second injection occurred the day of the acquisition, 3 h before the test; and then, the third injection occurred the day of the retention, 3 h before the test.

Subcellular fractionation. The DG isolation (Hagihara et al., 2009; Uchida et al., 2014) and subcellular fraction (Shumyatsky et al., 2005; Uchida et al., 2014) were performed as previously reported. For whole tissue lysates, freshly dissected tissues were homogenized in ice-cold RIPA buffer (50 mM Tris, pH 8.0, 1% Triton X-100, 0.1% SDS, 150 mM NaCl) containing protease and phosphatase inhibitor mixture tablets (Roche Applied Science). Synaptosomal fractionation was conducted using an adopted protocol with minor modifications (Uchida et al., 2014). In brief, pooled dissected tissues from the DG of 3 or 4 mice were homogenized in cold buffer containing 0.32 M sucrose, 50 mM sodium fluoride, and 10 mM HEPES, pH 7.4. Homogenates were cleared two times at 1000 × *g* for 10 min to remove nuclei and large debris. The resulting supernatants were passed through nitrocellulose filter (5 μm, Millipore) and were concentrated at 1000 × *g* for 20 min to obtain the synaptosomal fraction. Microtubule fractionation was performed as previously reported (Shumyatsky et al., 2005). In brief, the pooled dissected tissues from the DG of 3 or 4 mice were homogenized in 400 μl of microtubule stabilizing buffer MTSB (0.1 M PIPES, pH 6.9, 2 M glycerol, 5 mM $MgCl_2$, 2 mM EGTA, 0.5% Triton X-100, 4 μg/ml Paclitaxel, 5 μg/ml pefabloc SC, 5 μg/ml leupeptin) and ultracentrifuged at 32,000 × g for 20 min at 4°C. The resulting pellet was resuspended in the MTSB buffer. Nuclear fraction was purified using NE-PER Nuclear and Cytoplasmic Extraction Reagents (Thermo Scientific) according to the manufacturer's manual. To validate the isolated proteins, we performed Western blot with antibodies against histone H3 and synaptophysin for a nuclear protein and a synapse-enriched protein, respectively. We confirmed the expression of histone H3, but not synaptophysin, in nuclear fraction used in this study (data not shown). Protein concentration was measured by BCA protein assay (Thermo Scientific).

Western blotting. The DG was isolated as previously reported (Hagihara et al., 2009; Uchida et al., 2014). Western blotting was performed as previously reported (Uchida et al., 2011a, 2014). Equal amount of proteins were separated on 7% or 12% Bis-Tris gels (Invitrogen) and transblotted onto polyvinylidene difluoride membranes (GE Healthcare Bio-Sciences). After blocking the membrane with 5% skim milk or 5% BSA, the membranes were incubated with antibodies directed against β-actin (1:5000; Sigma), GAPDH (1:5000; Millipore), pS16-stathmin (1:1000, Cell Signaling), pS25-stathmin (1:1000, Abcam), pS38-stathmin (1:1000, Cell Signaling), total stathmin (1:5000, Millipore), histone H3 (1:4000; Cell Signaling), GluA1 (1:500; Millipore), GluA2 (1:500; Millipore), GluN1 (1:500; Millipore), GluN2A (1:500 Millipore), GluN2B (1:500; Millipore), CREB (1:500, Millipore), or pCREB (1:500, Millipore). After incubation with appropriate HRP-conjugated secondary antibodies (HRP-linked anti-mouse IgG or HRP-linked anti-rabbit IgG antibody, Cell Signaling), the blots were developed using the ECL-Plus Detection Kit (GE Healthcare Bio-Sciences or Thermo Scientific). When the phospho-specific antibodies were used, all buffers included sodium fluoride (50 mM). Densitometric analysis was performed by ImageQuant software (GE Healthcare) after scanning (Typhoon, GE Healthcare).

Real-time PCR. Quantitative real-time PCR was performed as reported previously (Uchida et al., 2010, 2011a). The total RNA from dissected tissues was extracted using RNeasy Mini Kit (QIAGEN) or TRIzol Reagent (Invitrogen) and treated with DNase (DNA-free kit, Ambion). The quality of the RNA (A_{260}/A_{280}) was 1.8–2.0 for all RNA preparations. The purified total RNA was used for cDNA synthesis using the Omniscript RT Kit (for QIAGEN, see Fig. 8) or TaqMan Gold RT-PCR kit (for Applied Biosystems, see Fig. 10). The cDNA was stored at −80°C until use. Real-time PCR was performed using the Applied Biosystems 7900HT Fast Real-Time PCR System with SYBR Green PCR master mix (Applied Biosystems) according to the manufacturer's protocol. The PCR conditions were 15 min at 95°C followed by 45 cycles of 15 s at 95°C and 30 s at 60°C. The following primers were used for quantitative PCR: *Gfp*, forward (5′-GCAGAAGAACGGCATCAAGGT-3′) and reverse (5′-CTTGTGGCCGAGAATGTTTC-3′); *c-fos*, forward (5′-ATGGGCTCTCCTGTCAACACAC-3′) and reverse (5′-ATGGCTGTCACCGTGGGGATAAAG-3′); *Arc*, forward (5′-TACCGTTAGCCCCTATGCCATC-3′) and reverse (5′-TGATATTGCTGAGCCTCAACTG-3′); *Gapdh*, forward (5′-CATGGCCTTCCGTGTTCCT-3′) and reverse (5′-TGATGTCATCATACTTGGCAGGTT-3′); and *β-actin*, forward (5′-CTGTCCACCTTCCAGCAGAT-3′) and reverse (5′-AGTCCGCCTAGAAGCACTTG-3′).

Amplification of a single PCR product was confirmed by monitoring the dissociation curve and by electrophoresis on 1.5% agarose gels stained with ethidium bromide. All measurements were performed in triplicate. *Glyceraldehyde-3-phosphate dehydrogenase (Gapdh)* mRNA levels were used to normalize the relative expression levels of target mRNAs. When a significant difference was observed between experimental groups, the data were further confirmed by normalizing to the other internal control, *β-actin*.

Chromatin immunoprecipitation (ChIP) assay. Dissected DG tissues were minced into 1 mm pieces that were immediately frozen on dry ice and stored at −80°C until further use. To crosslink the protein-DNA complexes, the tissues were placed in 1% formaldehyde for 15 min at room temperature. Fixation was quenched by adding glycine at a final concentration of 0.125 M. The tissues were washed three times with ice-cold PBS containing protease inhibitors (Complete Tab, Roche Diagnostics) and were homogenized with 12 strokes in 10 mM Tris, 10 mM NaCl, and 0.2% NP-40. The homogenate was centrifuged at 4500 × *g* for 5 min. The supernatant was removed, and the cell pellet was then homogenized 2 more times using nuclear lysis buffer (Millipore) containing protease inhibitors. Each sample was sonicated on ice, resulting in the formation of genomic DNA fragments (size: 200–1000 bp). The nuclear lysates were centrifuged at 16,000 × *g* for 20 min to remove insoluble material. The resulting lysates were then immunoprecipitated overnight at 4°C using 5 μg of an antibody directed against CREB (Millipore) or pCREB (Ser133, Abcam). All assays included normal rabbit IgG (Santa Cruz Biotechnology) and no-antibody immunoprecipitations to confirm the specificity of each antibody used. Chromatin-antibody complexes were collected using Protein G Magnetic Beads (Cell Signaling) and were sequentially washed 5 times with RIPA buffer and once with TE buffer containing 50 mM NaCl. Chromatin was eluted using $NaHCO_3$/SDS buffer. The ChIP, input (reserved from the precleared step), and negative control samples were incubated under high-salt conditions at 65°C overnight for crosslink reversal. The DNA fragments were then purified, and the DNA samples were subjected to quantitative real-time PCR analyses.

Contextual discrimination learning. All behavioral testing of adult male mice was performed during the light phase of the cycle. This test was performed as previously reported with minor modifications (Clement et

al., 2012; Nakashiba et al., 2012). Mice were trained to discriminate between two contexts through repeated experience in each. Context A consisted of four identical conditioning chambers. The side walls of each chamber were made of aluminum, whereas the back wall, front door, and ceiling were made of clear Plexiglas. The floor of each chamber consisted of stainless steel rods, which were wired to a shock generator and scrambler. The overhead fluorescent room lights remained on. This context was cleaned with 70% ethanol. Context B consisted of four chambers which had white plastic side walls. Similar to context A, the floor of each chamber consisted of stainless steel rods, which were wired to a shock generator and scrambler. The overhead fluorescent room lights remained on. This context was cleaned and scented with a 1% acetic acid solution. During the first 10 training sessions, mice were placed in context A and allowed to explore for 148 s before the delivery of shock (0.75 mA, 2 s). Mice were removed from the conditioning chamber 30 s after shock. Freezing was measured each day during the first 2 min baseline period by the FreezeView software (Coulbourn Instruments). After 10 sessions of conditioning in context A, mice underwent two sessions of generalization test. In the first session, mice were placed into the context A or context C for 3 min; and 2 h later, mice were placed in the opposite contexts for 3 min, with the order counterbalanced such that half of the animals were placed in context A first and half were placed in context C first. Context C had the same dimension as context A, but the chambers had a curved plastic wall and the flat plastic floor (no stainless steel rods). The chambers were cleaned with a lemon-scented solution. The room was lit with a red overhead light. In the second session, mice were placed into the context A or context B for 3 min; and 2 h later, mice were placed in the opposite contexts for 3 min, as described earlier. For discrimination learning, mice were exposed to the training context A in which they received a single 2 s foot shock of 0.75 mA at 148 s after placement in the chamber. Mice were taken out of the chamber 30 s after termination of the foot shock and returned to their home cage. After 2 h, mice were placed in the similar context B, in which they were left for 180 s and were never shocked. The order of exposure to context on each day was in an alternating fashion (i.e., B, A, A, B, B, A, A, B, B, A for first exposure through the 10 discrimination sessions). The freezing levels in both the training context (first 2 min) and the similar context (first 2 min) were measured.

Single-pairing fear conditioning. Single-pairing fear conditioning experiment was done as described previously (Shumyatsky et al., 2002, 2005). On the training day, the mouse was placed in the conditioning chamber (Med Associates) for 2 min before the onset of the tone (30 s, 2800 Hz, 85 dB). The last 2 s of the conditioned stimulus (CS) was paired with a foot shock (0.7 mA). After an additional 30 s in the chamber, the mouse was returned to its home cage. Twenty-four hours later, conditioning was assessed for 3 consecutive minutes in the chamber in which the mice were trained by scoring freezing behavior, which was defined as the complete lack of movement. Testing for contextual memory occurred in the context in which mice were trained. Three hours later to test memory for cued fear conditioning, mice were placed in a novel environment in which the tone (120 s) that had been presented during training was given after a 1 min habituation period (pre-CS). The time spent freezing was measured by the FreezeView software (Coulbourn Instruments).

Five-pairing paradigm, paired versus unpaired protocol. On the training day, the mouse was placed in the conditioning chamber (Med Associates) for 700 s during which the paired group received five shocks (0.7 mA, 50 Hz, 2 s) paired with the tone (2800 Hz, 30 s, 85 dB) with the intertrial interval ~70 s. The unpaired group stayed also 700 s in the conditioning chamber during which they received five pseudorandom tones (2800 Hz, 30 s, 85 dB) that were not contingent on delivery to the five shocks (0.7 mA, 50 Hz, 2 s). For both groups after the last tone, mice stayed in the box 1 min before going back to the home cage. Testing occurred 24 h later, and the procedure was identical for the paired and unpaired groups. Mice were first placed for 3 min in the context in which they were trained (contextual memory). The time spent freezing was measured as described above.

Unpaired fear conditioning with delayed retention. On the training day, the mouse was placed in the conditioning chamber (Med Associates) for 700 s during which the mouse received five pseudorandom tones (2800 Hz, 30 s, 85 dB) that were not contingent on delivery to the five shocks (0.7 mA, 50 Hz, 2 s). After the last tone, mice stayed in the box 1 min before going back to the home cage. Testing occurred 15 d later. Mice were first placed for 3 min in the context in which they were trained (contextual memory). The time spent freezing was measured as described above.

Upstairs/downstairs procedure. This test was performed as previously reported (Wiltgen et al., 2010). Mice were trained in two distinct environments: contexts A and B. Context A was cleaned with 1% acetic acid diluted in deionized water. In contrast, context B cleaned with 70% ethanol. On day 1, animals were trained in context A. After an initial 118 s baseline period, animals received three unsignaled footshocks (0.5 mA, 2 s) spaced 58 s apart and were removed 60 s after the last shock. On day 2, animals were trained in context B using the same protocol as day 1. The animals received 3 min tests on days 3 and 4 (no footshock) to assess fear in contexts B and A, respectively. The time spent freezing was measured as described above.

Open field test. This test was performed as previously reported (Martel et al., 2010). The open-field consisted of a white arena (43.2 cm × 43.2 cm × 40 cm) coupled to an automated video tracking system (Open Field Activity Software, Med Associates). Mice were placed in the corner of the arena, and the time spent in the peripheral area and the total distance traveled (locomotion) were measured. Results are expressed as the ratio of the time spent in the periphery over the total time spent in the arena.

Elevated plus maze. This test was performed as previously reported (Martel et al., 2010). The elevated plus maze (1 m above the floor) consisted of a center platform (10 cm × 10 cm), two open arms (40 cm × 10 cm), and two closed arms (40 cm × 10 cm) within walls (height 30 cm). Mice were placed individually in the center of the apparatus, and the time spent in each arm was measured for 5 min using Limelight software (Coulbourn Instruments). Results are expressed as the percentage of the time spent in closed arms over the total time spent in the maze.

Pain sensitivity. Response to the electric shock was assessed with naive mice as described previously (Shumyatsky et al., 2002; Martel et al., 2011). The intensity of the shock required for running, vocalization, and jump was determined for each mouse by delivering a 1-s-long shock every 30 s starting at 0.08 mA and increasing the shock 0.02 mA each time. Testing was stopped after all behaviors were noted.

Statistical analysis. Analyses of the data were performed using an appropriate ANOVA. Significant effects were followed up with Fisher's LSD, Tukey's *post hoc* test, or Bonferroni's correction. Student's *t* tests were used for two-group comparisons. In all cases, p values were two-tailed, and the comparisons were considered statistically significant when $p < 0.05$. All data are presented as mean ± SEM.

Results

Stathmin is abundantly expressed in the DG

We first characterized the expression of endogenous stathmin in adult and juvenile C57BL/6J mice. Immunohistochemistry with a specific antibody against stathmin revealed its strong expression in the DG, cortex, and amygdala in both adult and juvenile mice (Fig. 1*A–D*). We then investigated the cell types expressing stathmin in the DG. Immunofluorescence analysis illustrated that stathmin is expressed in both NeuN-positive mature neurons and DCX-positive immature neurons, but not in GFAP-positive astrocytes, in both adult and juvenile mice (Fig. 1*E*,*F*). In the CA1 and CA3 regions, stathmin immunofluorescence was observed in NeuN-positive neurons, but signals were weak (Fig. 1*G*,*H*). Quantification analyses revealed that stathmin is abundantly expressed in the subgranular zone of the DG compared with its expression in the granule cell layer as well as the CA1 and CA3 regions in adult and juvenile mice (Fig. 1*I*). In addition, stathmin expression in the subgranular zone of juvenile mice was greater than that in adult mice. Conversely, stathmin expression in the granule cell layer, CA1, and CA3 of juvenile mice was reduced compared with adult mice (Fig. 1*I*). Western blotting confirmed

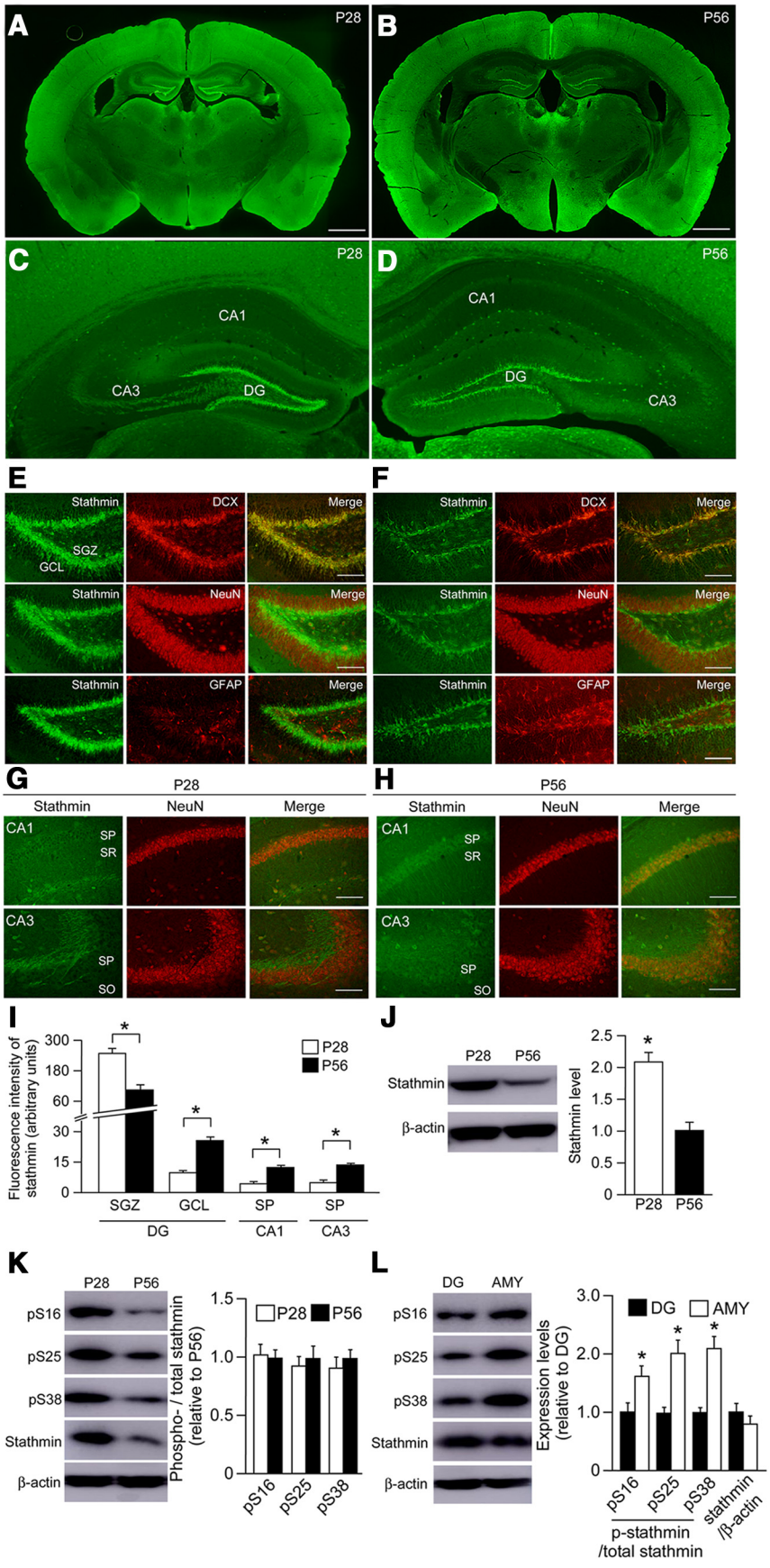

Figure 1. Characterization of endogenous stathmin expression in the mouse brain. ***A–D***, Endogenous stathmin is expressed abundantly in the DG, amygdala, and cortex in both adult (P28, ***A***, ***C***) and juvenile (P56, ***B***, ***D***) wild-type mice. Scale bar, 1 mm. ***E***, ***F***, Stathmin is expressed in both NeuN-positive mature and DCX-positive immature neurons, but not in GFAP-positive astrocytes, of the DG in both juvenile (***E***) and adult (***F***) WT mice. Antibodies against NeuN, GFAP, and DCX are used as markers for mature neurons, astrocytes, and immature neurons, respectively. Scale bar, 100 μm. ***G***, ***H***, Stathmin is expressed in NeuN-positive mature neurons in the CA1 and CA3 regions of juvenile (***G***) and adult (***H***) wild-type mice. Scale bar, 100 μm. ***I***, Quantification analyses of stathmin level in the selected brain subregion of adult and juvenile mice. $^*p < 0.05$. ***J***, Western blot showing the level of total stathmin in the DG of adult and juvenile mice. $^*p < 0.05$. ***K***, Western blot showing the level of *p*-stathmin (Ser16, Ser25, and Ser38) in the DG of adult and juvenile mice. ***L***, Western blot showing the level of *p*-stathmin (Ser16, Ser25, and Ser38) in the DG and amygdala in adult mice. $^*p < 0.05$. Data are mean ± SEM.

that the level of stathmin protein in the DG of juvenile mice is greater than that in adult mice (Fig. 1*J*). Overall, these results indicate that stathmin is enriched in the DG, suggesting a possible role for stathmin in controlling neurogenesis in this brain area.

Given that phosphorylation of stathmin leads to an increase in microtubule stability and a decrease in microtubule dynamics, we also measured the levels of *p*-stathmin (Ser16, Ser25, and Ser38) in the DG of adult and juvenile mice. Western blotting revealed that the signals of these three forms of *p*-stathmin are abundant in juvenile mice, but there were no statistical differences (Fig. 1*K*) due to the altered total stathmin level (Fig. 1*J*). We also compared stathmin levels between adult DG and amygdala tissue and found that levels of *p*-stathmin were lower in the DG compared with the amygdala (Fig. 1*L*). This suggests that dynamic microtubules might be more easily affected by overexpressing a stathmin transgene in the DG versus amygdala.

Characterization of transgene expression in *Stat4A* mice

We created the *Grp-tTA* knockin mouse (Uchida et al., 2014) and examined its tTA expression pattern by crossing it with the *tetO-LacZ* reporter mouse (Fig. 2*A*). Strong LacZ staining was observed in the DG and lateral amygdala with lighter staining in the basal amygdala and cortex (Fig. 2*B*). Because of the strong DG expression, we decided to use the *Grp-tTA* mouse line to examine the role of stathmin in adult hippocampal neurogenesis. Therefore, we developed *Stathmin4A* double mutant mice (*Stat4A* mice) using the *tTA/tetO* inducible bitransgenic system, which allows the *Stat4A* transgene to be activated and deactivated (Fig. 2*C*) (Uchida et al., 2014). The unphosphorylatable *Stat4A* gain-of-function mutant

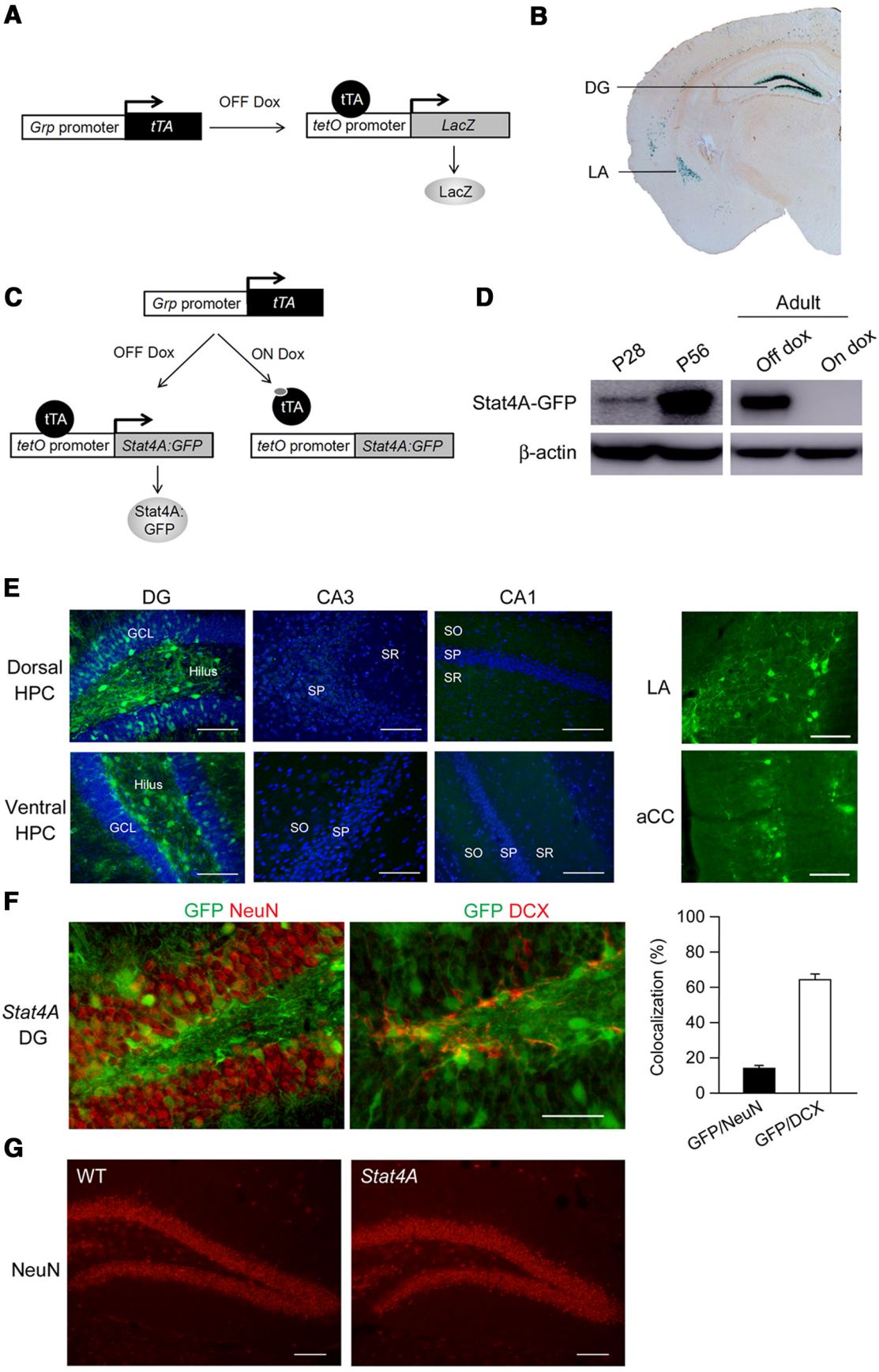

Figure 2. Characterization of transgene expression in *Stat4A* mice. ***A***, Diagram illustrating transgenic design for the *Grp-tTA x tetO-LacZ* reporter mice. ***B***, Expression pattern of LacZ in the *Grp-tTA x tetO-LacZ* reporter mice. ***C***, Diagram illustrating transgenic design and control of transgene expression by dox in the *Stat4A* mice. ***D***, Western blotting using anti-GFP antibody shows transgene expression in the DG at 28 (P28) and 56 (P56) days after birth (left) and that this expression is repressed by dox administration in the adult mouse (*Figure legend continues.*)

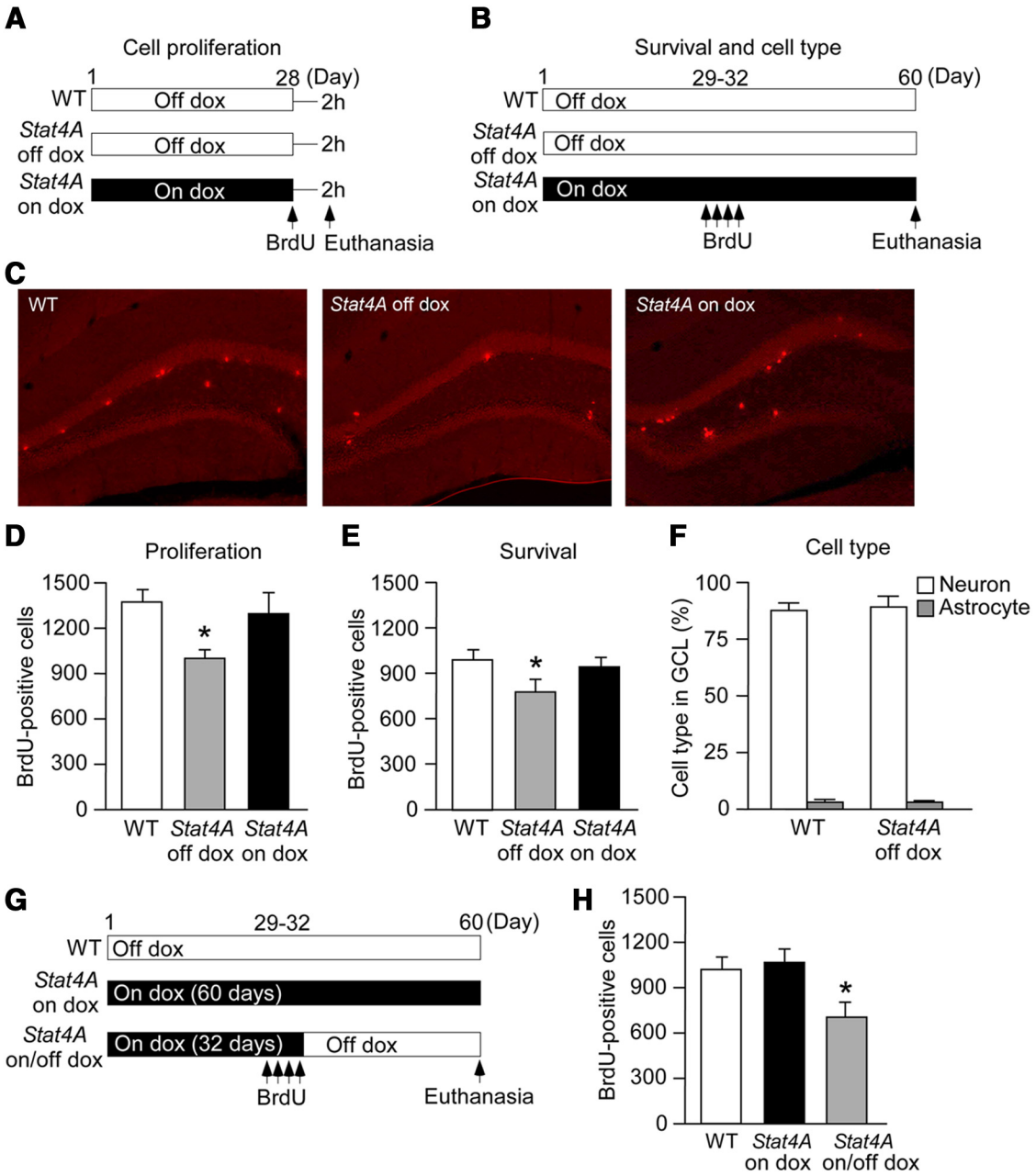

Figure 3. Reduced adult hippocampal neurogenesis in *Stat4A* mice. ***A***, ***B***, Experimental designs. BrdU was administered 2 h before death to examine the effects of *Stat4A* overexpression on cell proliferation (***A***). BrdU was administered once a day for 4 d, and mice were killed 4 weeks later to examine the effects of *Stat4A* overexpression on cell survival (***B***). The mice received a dox-containing food pellet for 4 weeks (***A***) and 60 d (***B***). ***C***, Images of BrdU staining (for cell proliferation) in the brain sections of adult *Stat4A* mice. ***D***, Reduced cell proliferation in adult *Stat4A* mice is prevented by dox administration. $n = 6$ in each group. $^*p < 0.05$ versus WT mice. ***E***, Reduced number of BrdU-positive cells in adult *Stat4A* mice is prevented by dox administration. $n = 6$ in each group. $^*p < 0.05$ versus WT mice. ***F***, Graph represents the percentages of BrdU-positive neurons and astrocytes in the granule cell layer. $n = 6$ in each group. ***G***, Experimental design. Adult *Stat4A* mice were fed dox-containing food pellets for 32 d and then fed normal food pellets for an additional 28 d (on/off dox mice). A different group of adult *Stat4A* mice was fed dox-containing food pellets for 60 d (on dox mice). BrdU was given once a day for 4 d, and mice were killed 4 weeks later to examine the effects of Stat4A overexpression on cell survival. ***H***, *Stat4A* on/off dox mice display fewer BrdU-positive cells. $n = 6$ in each group. $^*p < 0.05$ versus WT mice. Data are mean ± SEM.

←

(*Figure legend continued.*) (right). ***E***, Immunohistochemistry illustrates that the *Stat4A-GFP* transgene is expressed in the DG of the dorsal and ventral hippocampus, lateral amygdala (LA), and anterior cingulate cortex (aCC), but not in the CA1 or CA3 areas of the hippocampus. Scale bar, 200 μm. ***F***, Immunohistochemistry showing the *Stat4A-GFP* transgene expression in NeuN-positive mature neurons and DCX-positive immature neurons. Scale bar, 50 μm. ***G***, Immunohistochemistry using NeuN antibody reveals the normal gross anatomy of the DG in *Stat4A* mice. Scale bar, 100 μm. Data are mean ± SEM.

permanently binds α-tubulin, depleting cellular levels of free tubulin and destabilizing microtubules (Küntziger et al., 2001). The transgene is expressed in the DG of both adult and juvenile mice, and its expression is tightly regulated by dox (Fig. 2*D*). We also found that transgene expression in juvenile mutant mice was low compared with that in the DG of hippocampus of adult mice (Fig. 2*D*). Immunohistochemistry revealed that transgene expression is observed in the DG, but not in CA3 or CA1, of the dorsal and ventral hippocampus (Fig. 2*E*). The *Stat4A* transgene was also observed in the amygdala and anterior cingulate cortex of *Stat4A*

mice (Fig. 2*E*). In the DG, 13% of NeuN-positive mature neurons and 64% of DCX-positive immature cells expressed the transgene (Fig. 2*F*), suggesting that the majority of DCX-positive immature neurons express the *Stat4A* transgene. Expression of the transgene did not affect the gross anatomy of the DG in *Stat4A* mice (Fig. 2*G*). These results indicate that the use of *Stat4A* mice could allow us to examine the role of stathmin in DG neurogenesis.

Impaired adult hippocampal neurogenesis in *Stat4A* mice

To examine the effects of *Stat4A* overexpression on cell proliferation and survival, we performed BrdU staining (Fig. 3*A–E*). Relative to WT mice, *Stat4A* mice exhibited significantly fewer BrdU-positive cells in the subgranular zone of the DG 2 h after BrdU injection (Fig. 3*C*,*D*; $F_{(2,15)} = 4.041$, $p < 0.05$; Bonferroni's correction, WT vs *Stat4A* off dox, $p < 0.05$). The reduction of cell proliferation in *Stat4A* mice was prevented by dox administration for 4 weeks (Bonferroni's correction, WT vs *Stat4A* on dox, $p > 0.05$). Four weeks after BrdU injection, the number of BrdU-positive cells in the granule cell layer of the DG was significantly lower in *Stat4A* mice than in WT mice; this reduction was prevented when *Stat4A* mice were administered dox (Fig. 3*B*,*E*; $F_{(2,15)} = 5.096$, $p < 0.05$; Bonferroni's correction, WT vs *Stat4A* off dox, $p < 0.05$; WT vs *Stat4A* on dox, $p > 0.05$). In all groups, most BrdU-positive cells expressed the neuronal marker NeuN at 4 weeks (WT, 88%; Stat4A, 89%), whereas a small proportion of BrdU-positive cells were colabeled with the astrocyte marker GFAP at this time point (WT, 3%; Stat4A, 3%, Fig. 3*F*). No significant difference between genotypes was detected regarding these cell types in the DG granule neurons of newborns (Student's *t* test, $p > 0.05$).

We next performed a more detailed analysis of the effect of *Stat4A* overexpression on cell survival (Fig. 3*G*). *Stat4A* mice were fed with dox for 32 d and injected with BrdU during the last 4 d of dox treatment. During the 4 weeks following the last injection of BrdU, dox was removed (*Stat4A* on/off dox mice), and BrdU staining was performed. As previously shown, in *Stat4A* on/off dox mice, cell proliferation was normal when BrdU injections were performed (*Stat4A* on dox mice in Fig. 3*D*). Consequently, the specific effect of *Stat4A* overexpression on neuronal survival was assessed. The number of BrdU-positive cells in the granule cell layer of the DG was significantly lower in *Stat4A* on/off dox mice than in WT mice or *Stat4A* mice treated with dox for 60 d (Fig. 3*H*; $F_{(2,15)} = 11.353$, $p < 0.01$; Bonferroni's correction, WT vs *Stat4A* on dox, $p > 0.05$; WT vs *Stat4A* on/off dox, $p < 0.01$). Thus, *Stat4A* mice exhibited reduced neural progenitor proliferation and newborn neuron survival in the DG, suggesting that stathmin controls adult hippocampal neurogenesis.

Aberrant morphology of DG granule neurons in *Stat4A* mice

We examined the number of immature neurons in *Stat4A* mice using DCX immunohistochemistry. No change in the total number of DCX-positive cells was detected in *Stat4A* mice (Fig. 4*A*,*B*; $F_{(2,15)} = 0.312$; $p > 0.05$). DCX-positive cells were also subcategorized according to their dendritic morphology as follows: (1) DCX-positive cells with no tertiary dendritic processes; and (2) DCX-positive cells with complex, tertiary dendrites. We quantified the number of DCX-positive cells with tertiary dendrites as well as the maturation index (Wang et al., 2008; David et al., 2009). A reduced number of DCX-positive cells with tertiary dendrites (Fig. 4*C*; $F_{(2,15)} = 22.565$, $p < 0.01$; Bonferroni's correction, WT vs *Stat4A* off dox, $p < 0.01$; WT vs *Stat4A* on dox, $p > 0.05$) and a lower maturation index (Fig. 4*D*; $F_{(2,15)} = 8.453$, $p < 0.01$; Bonferroni's correction, WT vs *Stat4A* off dox, $p < 0.01$; WT vs *Stat4A* on dox, $p > 0.05$) were found in *Stat4A* mice compared with WT mice and *Stat4A* mice fed dox.

To investigate the dendritic morphology of mature granule neurons in the DG in adult *Stat4A* mice, we performed Golgi staining. The density of the dendritic spines of the DG granule neurons in *Stat4A* mice was decreased compared with that in WT mice (Fig. 4*E*; $F_{(2,21)} = 6.834$, $p < 0.01$; Bonferroni's correction, WT vs *Stat4A* off dox, $p < 0.01$). This reduction was prevented by feeding dox (Bonferroni's correction, WT vs *Stat4A* on dox, $p > 0.05$). The total dendritic length in *Stat4A* mice was normal (Fig. 4*F*; $F_{(2,21)} = 0.171$, $p > 0.05$). We did not see any differences in the spine density of the lateral amygdala neurons between *Stat4A* and WT mice (Fig. 4*G*). Thus, these data indicate that stathmin function is critical for spine morphology in the DG.

We also measured the total number of DCX-positive cells (Fig. 4*H*), number of DCX-positive cells with tertiary dendrites (Fig. 4*I*), and spine density (Fig. 4*J*) in DG granule neurons of juvenile *Stat4A* mice (4-week-old). We found that there were no significant effects on these phenotypes in juvenile *Stat4A* mice.

Stathmin activation leads to aberrant contextual fear discrimination learning

Current theories describe the DG as essential for the discrimination of two closely overlapping neural representations (Aimone et al., 2011), such as contextual discrimination, which is dependent on DG function (Leutgeb et al., 2007; McHugh et al., 2007). Neurogenesis in the DG appears to be critical for this type of discrimination (Sahay et al., 2011; Nakashiba et al., 2012). Consequently, the context discrimination paradigm becomes a powerful tool to link improper DG function to abnormal adult cognition. To examine context discrimination in *Stat4A* mice, mice were first trained in a fear conditioning paradigm for 10 d in unique context A (days 60–69). After acquisition training, mice were tested for generalization (days 70–71) and then exposed to the original training (context A). Finally, mice were exposed to the slightly different context B (days 72–81) (Fig. 5*A*). *Stat4A* mice were fed with dox for 2 months before the start of the conditioning. During the acquisition training, all of the mice learned the procedure ($F_{(9,399)} = 59.884$, $p < 0.001$), but *Stat4A* mice tended to display reduced contextual fear memory on days 61–64 without reaching significance (Fig. 5*B*; $p > 0.05$). During the test of contextual specificity (days 70–71), both *Stat4A* and WT mice were able to distinguish a pair of different contexts, A and C (Fig. 5*C*; $F_{(1,79)} = 171.27$, $p < 0.001$). Both genotypes exhibited robust and equivalent generalization between contexts, and no differences in freezing were observed ($p > 0.05$). The mice were subsequently trained to discriminate these contexts by visiting the two similar contexts A and B daily for 10 d. WT mice were able to discriminate between contexts A and B, as they learned to freeze less in context B (Fig. 5*D*; context effect, $F_{(1,139)} = 15.956$, $p < 0.01$; Fisher's LSD *post hoc* test on block 5, $p < 0.01$). By contrast, *Stat4A* mice were unable to discriminate between the two contexts over the same period ($F_{(1,139)} = 1.393$, $p > 0.05$). This deficit was prevented by feeding dox (context effect, $F_{(1,119)} = 6.210$, $p < 0.05$; Fisher's LSD *post hoc* test on block 5, $p < 0.05$).

Stathmin activation leads to deficits in contextual fear memory

We next investigated the effect of Stat4A overexpression on contextual and cued fear memories using a single tone-shock pairing for fear conditioning. *Stat4A* mice froze less during the context test 24 h after training (Fig. 6*A*; $F_{(2,39)} = 4.924$; $p < 0.05$; Fisher's LSD *post hoc* test WT vs *Stat4A*, $p < 0.01$). The impairment of

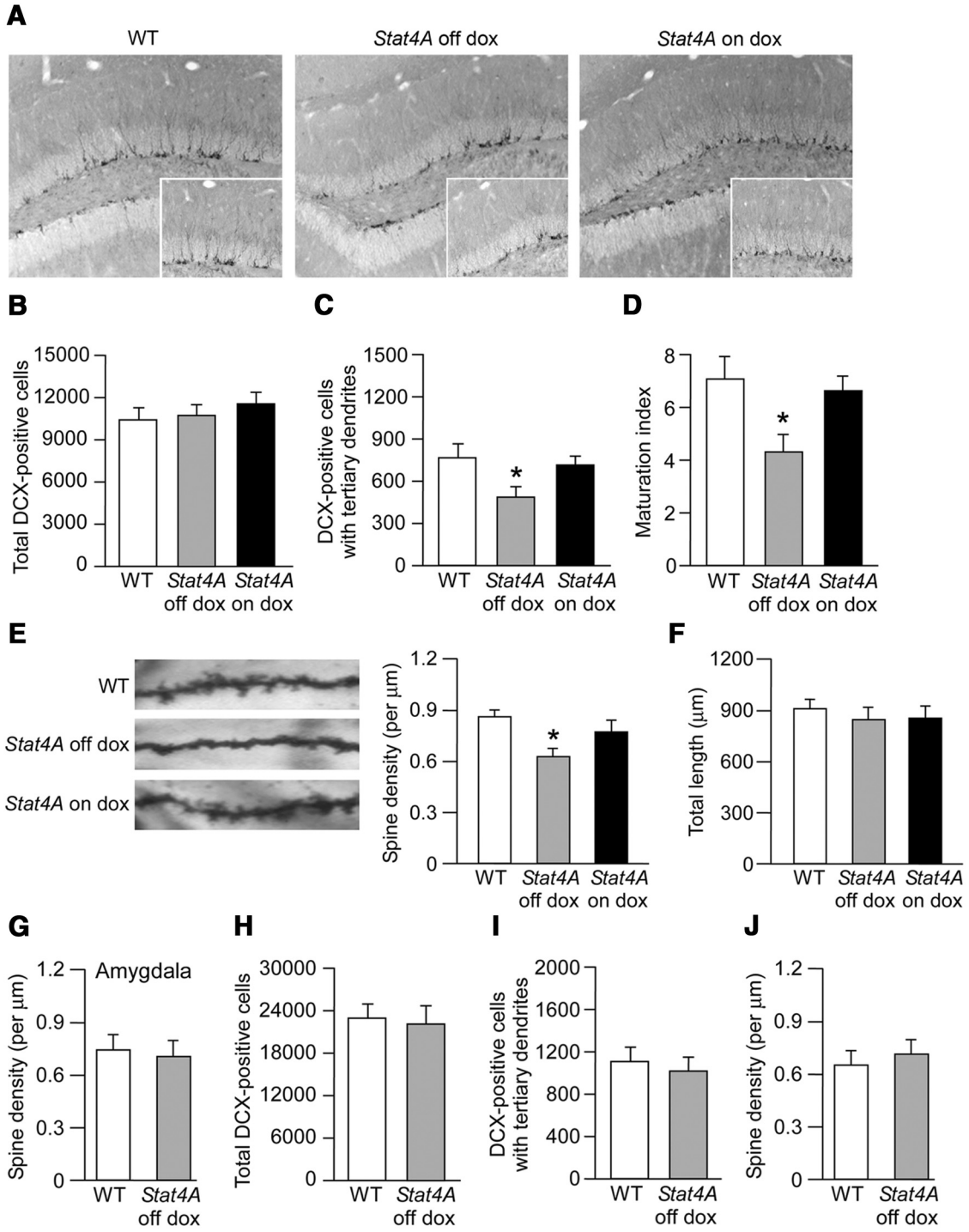

Figure 4. Immature DG in adult *Stat4A* mice. ***A***, Images of DCX staining in brain sections of *Stat4A* with or without dox mice. Insets, High-magnification images of DCX-positive cells. ***B***, Effect of *Stat4A* overexpression on the total number of DCX-positive cells. $n = 6$ for each group. ***C***, Reduced number of DCX-positive cells with tertiary dendrites in *Stat4A* mice is prevented by dox administration. $n = 6$ for each group. $^*p < 0.05$ versus WT mice. ***D***, Reduced maturation index of newborn granule cells in *Stat4A* mice. $n = 6$ for each group. $^*p < 0.05$ versus WT mice. ***E***, Reduced spine density of the DG granule neurons in *Stat4A* mice is prevented by dox administration. $n = 8$ for each group. $^*p < 0.05$ versus WT mice. ***F***, Normal dendritic length of the DG granule neurons in *Stat4A* mice. ***G***, Normal spine density of the lateral amygdala neurons in adult *Stat4A* mice. $n = 5$ for each group. ***H***, Effect of *Stat4A* overexpression on the total number of DCX-positive cells in juvenile mice (P28). $n = 5$ for each group. ***I***, Effect of *Stat4A* overexpression on DCX-positive cells with tertiary dendrites in juvenile mice. $n = 5$ for each group. ***J***, Normal spine density of the DG granule neurons in juvenile *Stat4A* mice. $n = 5$ for each group. Data are mean ± SEM.

contextual fear memory was prevented by feeding dox for 3 weeks (Fisher's LSD *post hoc* test WT vs *Stat4A* on dox, $p > 0.05$). During the tone test in a different context, all groups of mice froze similarly during the tone (Fig. 6*B*; $p > 0.05$). These results strongly suggest that *Stat4A* mice have deficits in contextual, but not cued, fear memory.

To further explore the deficit in contextual fear conditioning, *Stat4A* mice were tested in the five-tone-shock-pairings paradigm, which uses two procedures allowing for distinguishing between hippocampus-dependent memory (context in the foreground) and amygdala-dependent memory (context in the background) (Desmedt et al., 1998; Calandreau et al., 2005; Tri-

filieff et al., 2006). One procedure promotes an elemental association between the conditioned tone stimulus (CS) and the unconditioned stimulus (US foot shock; paired protocol) and requires minimal hippocampal contribution. In contrast, the second procedure favors hippocampal processing to support contextual conditioning by systematically minimizing CS/US contingency (unpaired protocol) (Kim and Fanselow, 1992; Desmedt et al., 1998; Desmedt et al., 2003).

In agreement with the previous studies, WT mice that were trained using the unpaired protocol (which favors hippocampal processing) froze significantly more to the training context than WT mice trained using the paired protocol (which decreases hippocampal contribution) (Fig. 6*C*; Fisher's LSD *post hoc* test, paired WT vs unpaired WT, $p < 0.05$). By contrast, *Stat4A* mice had a low level of freezing to the context regardless of the training protocol used (paired or unpaired) (Fig. 6*C*; Fisher's LSD *post hoc* test, paired *Stat4A* vs unpaired *Stat4A*, $p > 0.05$). In cued fear conditioning, all of the groups froze significantly more during the tone ($F_{(1,40)} = 101.993$; $p < 0.001$) but froze differently according to the type of training (paired vs unpaired) (Fig. 6*D*; $F_{(1,40)} = 15.274$, $p < 0.001$).

To eliminate the possibility that the specific deficit in contextual fear memory was due to the effects of anxiety and pain sensitivity, open field and elevated plus maze tests were performed, and responses to electric footshock were evaluated. *Stat4A* mice exhibited normal anxiety behaviors and locomotor activity in open field (Fig. 7*A*,*B*; $p > 0.05$) and in elevated plus maze tests (Fig. 7*C*; $p > 0.05$). In addition, *Stat4A* mice displayed normal pain sensitivity to electric footshock (Fig. 7*D*; $p > 0.05$). These results suggest that the observed deficits in fear conditioning were not related to sensitivity to footshock or innate anxiety.

We evaluated whether the deficit observed in fear conditioning could be due to possible positional effects following DNA insertions of the *tTA* or *tetO-Stat4A:GFP* transgenes. Single lines (*GRP-tTA* knockin, and *tetO-Stat4A:GFP* mice) displayed intact contextual fear memory (Fig. 7*E*; $p > 0.05$). We further tested the developmental effect of Stat4A overexpression on fear memory. We used a single pairing protocol for fear conditioning in adult *Stat4A* mice treated with dox during the developmental period (*Stat4A* on/off dox mice; Fig. 7*F*). Mothers were fed

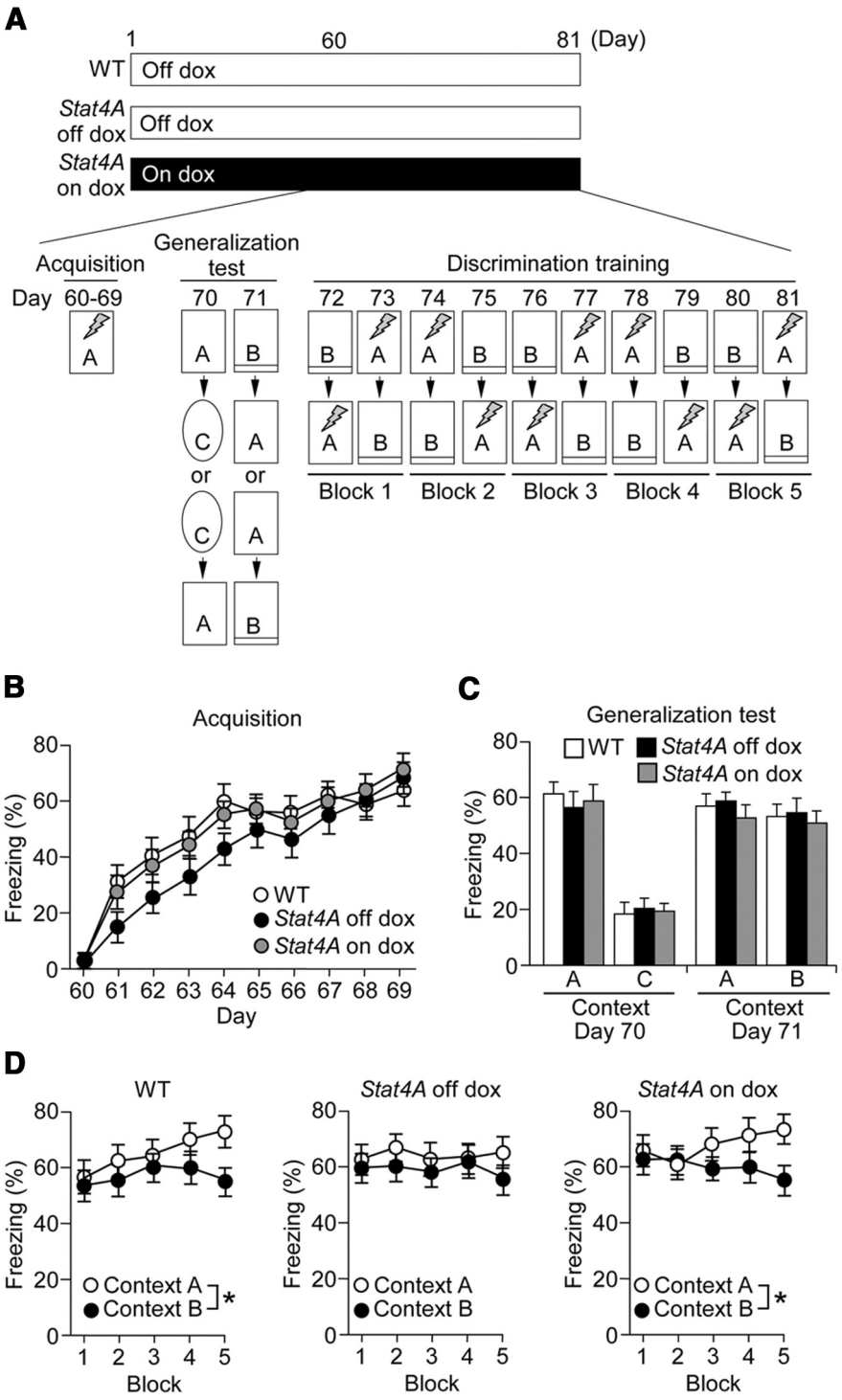

Figure 5. Impaired contextual fear discrimination learning in *Stat4A* mice. ***A***, Experimental design. We used three groups of mice: WT ($n = 14$), *Stat4A* mice without dox (*Stat4A* off dox, $n = 14$), and *Stat4A* mice administered dox for 2 months and during behavioral tests (*Stat4A* on dox, $n = 12$). Mice were trained in context A for 10 consecutive days. Subsequently, mice were subjected to a generalization test. In this test, mice were placed in training context A followed by context C or vice versa, and freezing was measured. On the next day, mice were placed in training context A followed by context B, which is slightly different from context A, or vice versa, and the freezing response was measured. Mice did not receive electric footshock during the generalization test. Next, mice were subjected to discrimination training for 10 consecutive days. During this test, mice were placed in context A and subsequently placed in context B or vice versa. When mice were placed in context A, electric footshock was applied, whereas no footshock was applied in context B. Freezing was measured in both chambers. ***B***, Freezing levels during the acquisition training. ***C***, Freezing levels in context A and the extremely different context C (day 70) or context A and slightly different context B (day 71) during the generalization test. ***D***, Freezing levels in contexts A and B during the discrimination training. Data are mean ± SEM. *$p < 0.05$.

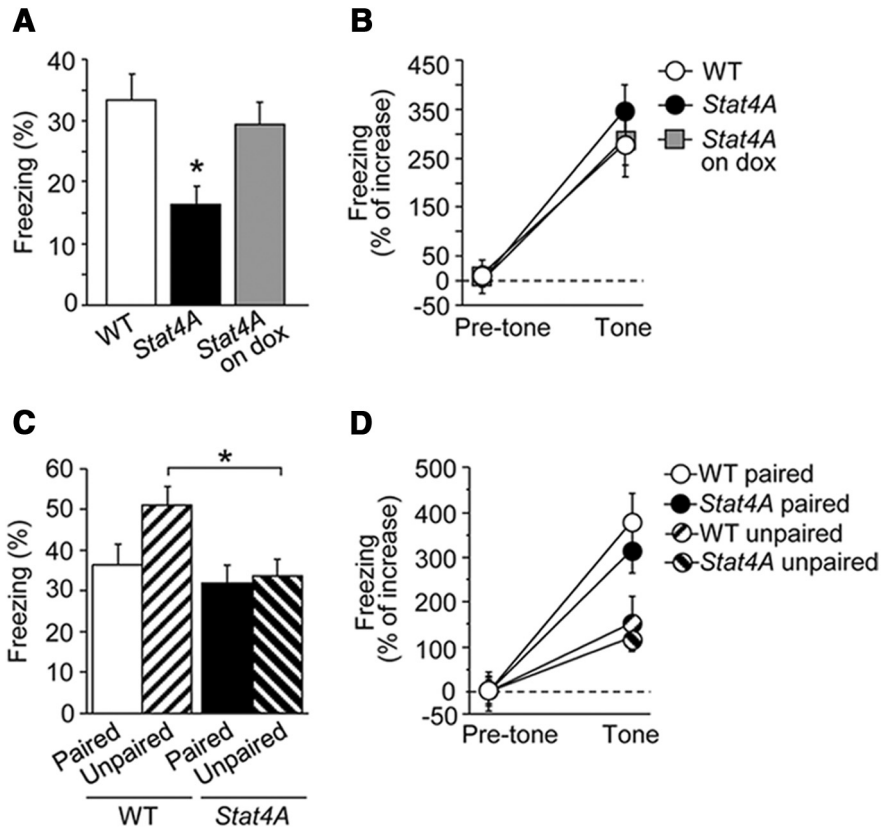

Figure 6. Impaired contextual fear memory in *Stat4A* mice. ***A***, ***B***, Single pairing fear conditioning test. Reduced contextual fear memory in *Stat4A* mice is prevented by dox administration (***A***). No significant difference in cued fear memory between *Stat4A* and WT mice (***B***). $n = 12–16$ for each group. $^*p < 0.05$ versus WT mice. ***C***, ***D***, Five tone-shock presentations with paired or unpaired protocol. Reduced contextual fear memory in *Stat4A* mice for the unpaired protocol but not the paired protocol (***C***). There is no significant effect of genotype in cued fear conditioning with the paired or unpaired protocol (***D***). $n = 12–16$ for each group. $^*p < 0.05$. Data are mean ± SEM.

dox during the pregnancy and postpartum periods until the testing mice were weaned at the age of 24 d. *Stat4A* mice were then fed with regular food and tested in a dox-free environment. *Stat4A* on/off mice exhibited impaired contextual fear memory (Fig. 7*G*; Student's *t* test, $p < 0.05$), similarly to *Stat4A* mice that were never administered dox. These results demonstrate that the deficit in contextual fear memory in *Stat4A* mice was not due to developmental effects induced by the presence of the *Stat4A* transgene.

Intrahippocampal injection of dox prevents the reduction of contextual fear memory in *Stat4A* mice

As the *Stat4A* transgene is expressed in both the DG and amygdala of *Stat4A* mice, we decided to inject dox specifically into the hippocampus or basolateral amygdala to determine which brain structure is responsible for the memory deficits. Immunohistochemistry revealed that transgene (*Stat4A*::GFP) expression was repressed by daily intrahippocampal injections of dox for 3 d (Fig. 8*A*,*B*; Student's *t* test, $p < 0.01$). Real-time PCR also confirmed that GFP mRNA expression was downregulated by intrahippocampal dox injection (Fig. 8*C*; Student's *t* test, $p < 0.01$). Single tone-shock pairing for fear conditioning revealed that impaired contextual fear memory in *Stat4A* mice was prevented by the intrahippocampal injection of dox (Fig. 8*D*; $F_{(2,31)} = 6.934$, $p < 0.01$; Fisher's LSD *post hoc* test WT vs *Stat4A*, $p < 0.01$; *Stat4A* vs *Stat4A* on dox, $p < 0.01$). Dox injected into the basolateral amygdala repressed transgene expression at both the protein (Fig. 8*E*,*F*; Student's *t* test, $p < 0.05$) and mRNA levels (Fig. 8*G*; Student's *t* test, $p < 0.05$). However, in contextual fear conditioning, freezing in *Stat4A* mice in which dox was injected into the basolateral amygdala was comparable with that in *Stat4A* mice injected with PBS (Fig. 8*H*; $p > 0.05$). Cannula replacements in these experiments are shown in Figure 8*I*, *J*. To rule out a possible effect of dox on fear memory, we injected dox or PBS into the hippocampus of WT mice and performed contextual fear conditioning. We did not find any differences in contextual and cued fear memories between PBS- and dox-injected mice (Fig. 8*K*,*L*; $p > 0.05$). Together, these behavioral results strongly suggest that stathmin's function in the DG is critical for contextual fear memory.

To determine which memory phase (i.e., acquisition or retrieval) is impaired in *Stat4A* mice, we tested Stat4A mice in a 15 d delayed retention unpaired fear conditioning paradigm (Fig. 9*A*). Four groups of mice were used: (1) WT mice without dox (WT off dox); (2) *Stat4A* mice fed dox for 15 d and then untreated for 15 d (*Stat4A* on/off dox); (3) *Stat4A* mice untreated for 15 d and then fed dox for 15 d (*Stat4A* off/on dox); and (4) untreated *Stat4A* mice (*Stat4A* off dox). During the context test, *Stat4A* on/off, off/on, and off mice froze significantly less than WT mice (Fig. 9*B*; $F_{(3,44)} = 5.327$, $p < 0.01$; Fisher's LSD *post hoc* test, WT off dox vs *Stat4A* on/off dox, $p < 0.01$; WT off dox vs *Stat4A* off/on dox, $p < 0.001$; WT off dox vs *Stat4A* off dox, $p < 0.01$), whereas genotype had no observable effect during the tone test (Fig. 9*C*). These results demonstrate that stathmin function in the DG is involved in both the acquisition and retrieval of contextual fear.

Stathmin affects NMDAR-mediated CREB-dependent transcription

We next examined the molecular mechanism underlying stathmin-mediated memory formation. The NMDAR is essential for synaptic plasticity and memory formation (Tsien et al., 1996; Tang et al., 1999; Lee and Silva, 2009). In addition, NMDAR function is thought to be linked to hippocampal neurogenesis (Nacher and McEwen, 2006; Tashiro et al., 2006). It should be noted that synaptic plasticity and memory are influenced by the transport of NMDARs along microtubules in neuronal dendrites (Yuen et al., 2005; Yin et al., 2011). Consequently, we hypothesized that altered NMDAR function could cause deficits in neurogenesis and memory in *Stat4A* mice. To test this hypothesis, we measured the levels of NMDARs (GluN1, GluN2A, and GluN2B), as well as AMPA receptors (GluA1 and GluA2) in the synaptosomal fraction from the DG in naive *Stat4A* mice. The amount of GluN2A and GluN2B in *Stat4A* mice was significantly decreased compared with WT and *Stat4A* mice fed dox (Fig. 10*A*; $F_{(2,15)} = 6.893$, $p < 0.01$; Bonferroni's correction, WT vs *Stat4A* off dox, $p < 0.05$; WT vs *Stat4A* on dox, $p > 0.05$; and $F_{(2,15)} =$

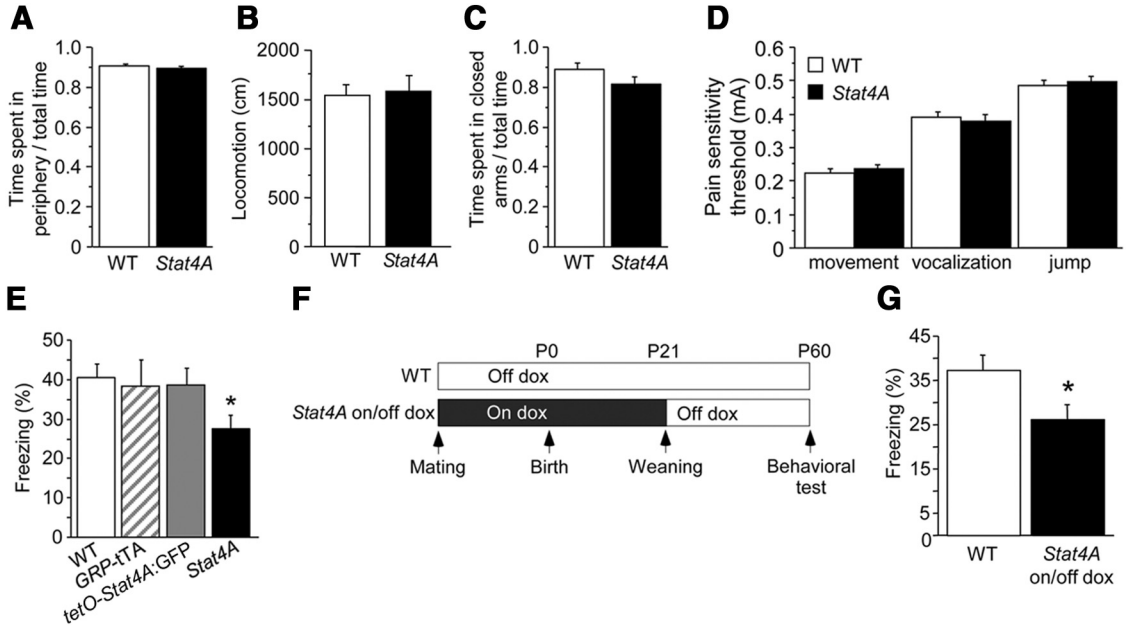

Figure 7. *Stat4A* mice have normal innate fear and shock sensitivity. ***A***, ***B***, There was no difference in the time spent in the periphery (***A***) or in locomotor activity (***B***) between *Stat4A* ($n = 16$) and WT mice ($n = 16$) in the open field. ***C***, There was no difference in the time spent in closed arm between *Stat4A* ($n = 16$) and WT mice ($n = 15$) in the elevated plus maze. ***D***, There was no difference in pain sensitivity between *Stat4A* ($n = 10$) and WT mice ($n = 10$). ***E***, Contextual fear memory was normal in both single mutant mouse lines ($n = 12$ per group), whereas *Stat4A* mice ($n = 12$) exhibited reduced freezing compared with WT mice ($n = 12$). $^*p < 0.05$. ***F***, ***G***, No developmental effects in contextual fear conditioning in *Stat4A* mice. ***E***, Experimental design. *Stat4A* mice were treated with dox until weaning (*Stat4A* on/off dox mice). The behavioral test was conducted during adulthood (2 months old). ***F***, Contextual fear memory in *Stat4A* on/off mice is decreased compared with that in WT mice. $n = 12$ for each group. $^*p < 0.05$. Data are mean ± SEM.

10.019, $p < 0.01$; Bonferroni's correction, WT vs *Stat4A* off dox, $p < 0.05$; WT vs *Stat4A* on dox, $p > 0.05$, respectively, for GluN2A and GluN2B). By contrast, no significant difference in GluN2A and GluN2B levels was detected in whole DG extracts among the groups (Fig. 10*B*; $p > 0.05$). In addition, the amount of GluN2A and GluN2B was significantly decreased in the microtubule fraction from the DG of *Stat4A* mice (Fig. 10*C*; $F_{(2,15)} = 5.632$, $p < 0.05$; Bonferroni's correction, WT vs *Stat4A* off dox, $p < 0.05$; WT vs *Stat4A* on dox, $p > 0.05$ and $F_{(2,15)} = 4.354$, $p < 0.05$; Bonferroni's correction, WT vs *Stat4A* off dox, $p < 0.05$; WT vs *Stat4A* on dox, $p > 0.05$, respectively, for GluN2A and GluN2B). No differences were detected in the expression levels of other subunits of NMDARs and AMPARs, namely, GluN1, GluA1, and GluA2, in the DG synaptosomal fraction and whole extracts among the groups (Fig. 10*A*,*B*; $p > 0.05$). We also examined the levels of NMDARs in synaptosomal and whole-cell extracts from the DG of juvenile (4-week-old) wild-type and *Stat4A* mice to see the developmental effect of *Stat4A* overexpression. We found that there were no significant effects of *Stat4A* overexpression on the levels of NMDARs in synaptosomal and whole-cell extracts (Fig. 10*D*). Overall, these results demonstrate that the transport of GluN2A and GluN2B from the cytosol to the synapse along with microtubules is altered in adult *Stat4A* mice.

To investigate the mechanism by which downstream targets of NMDARs are altered in *Stat4A* mice, we measured levels of phosphorylated CREB (pCREB, phosphorylated at Ser133), which can be induced through NMDAR activation (Lonze and Ginty, 2002; West et al., 2002; Zhu et al., 2002). Western blotting revealed that *Stat4A* mice had weakened but significant induction of pCREB at 30 min after fear conditioning compared with naive mice (Student's *t* test, $p < 0.05$), whereas both WT mice and *Stat4A* mice fed with dox exhibited strong pCREB induction (Fig. 10*E*; Student's *t* test, $p < 0.01$). To further examine the transcriptional control mediated by CREB, the mRNA levels of immediate early genes (*c-fos* and *Arc*) were evaluated 30 min after contextual fear conditioning acquisition. Real-time PCR revealed that mRNA levels for *c-fos* and *Arc* in the DG of *Stat4A* mice were significantly decreased compared with those in WT mice and dox-administered *Stat4A* mice (Fig. 10*F*,*G*; $F_{(2,89)} = 8.834$, $p < 0.001$; Bonferroni's correction, WT vs *Stat4A* at 30 min, $p < 0.001$; and $F_{(2,89)} = 7.276$, $p < 0.01$; Bonferroni's correction, WT vs *Stat4A* at 3 min, $p < 0.01$). To more directly investigate the effect of *Stat4A* overexpression on CREB-mediated gene transcription, we performed a ChIP assay. We found that pCREB was enriched at the *c-fos* promoter following learning in WT mice ($p < 0.05$), whereas Stat4A mice had no effect ($p > 0.05$; Fig. 10*H*). The levels of total CREB occupancy at the *c-fos* promoter were comparable between WT and *Stat4A* mice (Fig. 10*I*). These results are suggestive of aberrant CREB-mediated gene transcription following learning in *Stat4A* mice.

Stathmin does not affect NMDAR-independent memory

The results of the present study clearly demonstrate that overexpression of mutant *Stat4A* leads to dysfunction of NMDARs, which might be a causal mechanism for impaired learning and memory. To validate this hypothesis, we performed contextual fear conditioning using the "upstairs/downstairs" procedure (Wiltgen et al., 2010) to examine NMDAR-independent memory in *Stat4A* mice (Fig. 11*A*). In this task, an initial learning event was conducted on day 1 (context A; "upstairs"), and a subsequent learning event was conducted in a different environment the next day (context B; "downstairs"). Mice were then tested for freezing in contexts B and A on days 3 and 4, respectively. The NMDAR antagonist

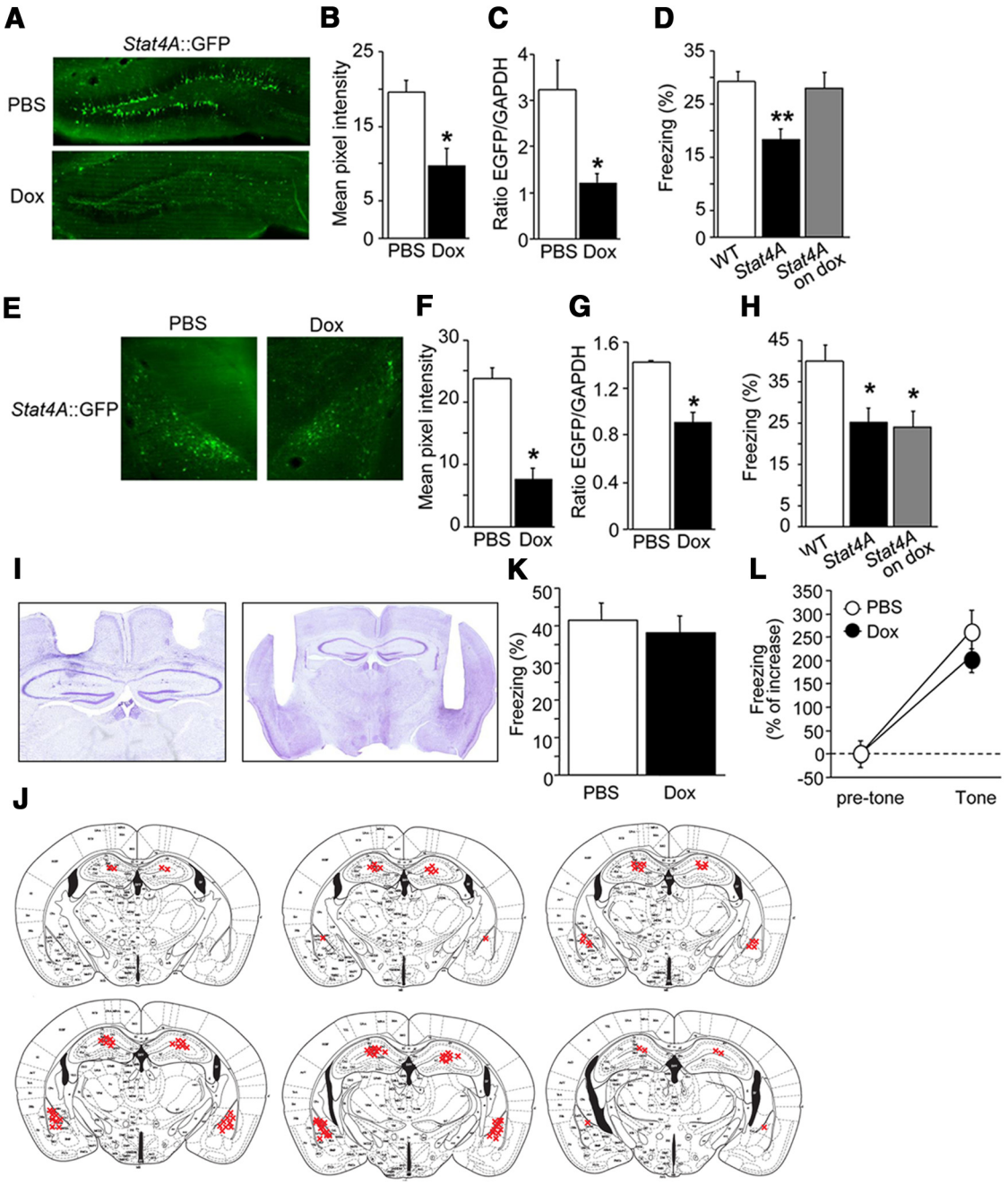

Figure 8. Local dox infusions in the hippocampus, but not in the amygdala, prevent deficits in fear conditioning. ***A***, ***B***, Representative images of GFP immunohistochemistry in the hippocampal sections of *Stat4A* mice in which dox was injected into the hippocampus (***A***). Intrahippocampal injection of dox reduces GFP immunoreactivity in *Stat4A* mice (***B***). $n = 9–12$ for each group. $^*p <$ 0.05. ***C***, Real-time PCR revealing reduced *gfp* mRNA in the hippocampus of *Stat4A* mice injected with dox. $n = 9–12$ for each group. $^*p < 0.05$. ***D***, Intrahippocampal injection of dox rescues contextual fear memory in *Stat4A* mice. $n = 9–12$ for each group. $^{**}p < 0.01$ versus WT mice. ***E***, ***F***, Representative images of GFP immunohistochemistry in the amygdala sections of *Stat4A* mice in which dox was injected into the lateral amygdala (***E***). Intralateral amygdala injection of dox reduces GFP immunoreactivity in *Stat4A* mice (***F***). $n = 9–12$ for each group. $^*p < 0.05$. ***G***, Real-time PCR reveals reduced GFP mRNA in the amygdala of *Stat4A* mice injected with dox. $n = 9–12$ for each group. $^*p < 0.05$. ***H***, Intralateral amygdala injection of dox does not rescue contextual fear memory in *Stat4A* mice. $n = 9–12$ for each group. $^*p < 0.05$ versus WT mice. ***I***, Representative images show the placements of guide cannulae in the dorsal hippocampus (left) and lateral amygdala (right). ***J***, Cannula tip placements from mice infused with dox. ***K***, Normal contextual fear memory in WT mice in which dox was injected into the hippocampus. $n = 9$ per group. ***L***, Normal cued fear memory in WT mice in which dox was injected into the hippocampus. $n = 9$ per group. Data are mean ± SEM.

CPP was effective at blocking learning in context A but not in context B, indicating that memory for context A is NMDAR-dependent but that for context B is independent of NMDAR (Wiltgen et al., 2010). *Stat4A* mice exhibited normal freezing in context B ($p > 0.05$) and reduced freezing in context A (Fig. 11*B*; Student's *t* test, $p < 0.05$), suggesting that *Stat4A* mice display normal NMDAR-independent memory. These results support our hypothesis that stathmin is involved in the regulation of NMDARs and therefore in memory formation.

Discussion

We found reduced cell proliferation and cell survival in the DG of adult *Stat4A* mice, suggesting that stathmin plays an important role in regulating adult hippocampal neurogenesis. A previous report

indicated that stathmin is enriched in immature DG neurons (Jin et al., 2004; Boekhoorn et al., 2014), confirming our immunohistochemical characterization of stathmin. We further characterized the role of stathmin in DCX-positive immature neurons, as our immunohistochemical evidence revealed that endogenous stathmin is highly expressed in DCX-positive cells. We found that the maturation index of DCX-positive cells is decreased in *Stat4A* mice. Moreover, Golgi staining revealed that the spine density of DG granule neurons is reduced in *Stat4A* mice. Although previous reports indicate that stathmin regulates cell growth, differentiation, maturation, and cell cycle progression in both cultured cells (Sobel, 1991; Curmi et al., 1999; Ohkawa et al., 2007a) and mouse cerebellar dendrites (Ohkawa et al., 2007b), the neurobiological roles of stathmin in the adult mouse hippocampus remained unclear. It should be noted that the induction of long-term potentiation is impaired in the DG of *Stat4A* mice (Uchida et al., 2014). Together with these results, our findings suggest that the DG stathmin plays an important role in structural and synaptic plasticity.

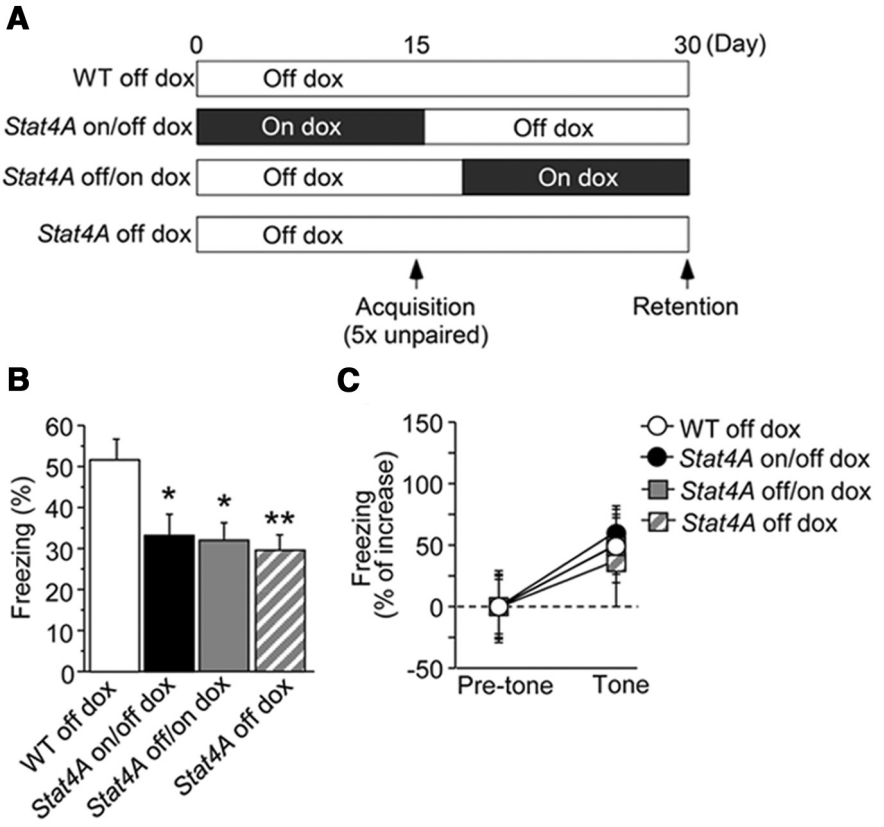

Figure 9. Stathmin is involved in both the consolidation and retrieval of memory in contextual fear conditioning. ***A***, Experimental design. ***B***, All groups of *Stat4A* mice froze significantly less than WT mice in the context test. $n = 12$ for each group. $^{*}p < 0.05$ versus WT off dox mice. $^{**}p < 0.001$ versus WT off dox mice. ***C***, There was no significant difference in cued fear memory among the groups. Data are mean ± SEM.

Hippocampal neurogenesis is reported to contribute to contextual discrimination (Sahay et al., 2011; Nakashiba et al., 2012). Although the molecular mechanisms underlying contextual discrimination remain to be understood, NMDARs appear to play an important role. In agreement with earlier work that demonstrates that the deletion of GluN2B-containing NMDARs from granule cells impairs contextual fear discrimination (Kheirbek et al., 2012), we have shown that *Stat4A* mice exhibit deficits in this task and decreased expression of synaptosomal GluN2B. Given that NMDARs are implicated in neurogenesis and spine formation (Nacher and McEwen, 2006; Tashiro et al., 2006; Hamilton et al., 2012), our data suggest that deficits in synaptic NMDAR localization caused by stathmin mutation lead to impaired hippocampal neurogenesis and maturation of DCX-positive cells, which in turn negatively regulate discrimination learning.

We also found that *Stat4A* mice display deficits in contextual fear memory, but not in cued fear memory, in two different behavioral paradigms (single pairing and unpaired-paired protocols), suggesting impaired hippocampus-dependent memory in *Stat4A* mice. Indeed, intrahippocampal injections of dox prevented a deficit in contextual fear memory in *Stat4A* mice, whereas intra-amygdala injections of dox did not affect memory. Furthermore, *Stat4A* mice exhibited deficits in spatial learning in the Morris water maze and Barnes maze, both of which are dependent on the hippocampus (Morris et al., 1982; Bach et al., 1995). These results further support the notion that *Stat4A* mice have an impairment in hippocampus-dependent memory. Both increasing and decreasing adult neurogenesis affects hippocampus-dependent memories, although these results have been somewhat controversial (Deng et al., 2010). Changes in adult neurogenesis influenced contextual fear memory and spatial learning and memory in some studies (Saxe et al., 2006; Imayoshi et al., 2008; Zhang et al., 2008b; Clelland et al., 2009; Guo et al., 2011; Pan et al., 2012) but not in others (Meshi et al., 2006; Denis-Donini et al., 2008; Zhang et al., 2008a; Deng et al., 2009). These contradictory results may be due to several reasons, including different experimental approaches and behavioral conditions (Pan et al., 2012; Frankland, 2013). In our experiments, repression of the transgene by chronic treatment with dox in *Stat4A* mice rescued neurogenesis and spinogenesis as well as contextual fear memory, suggesting that decreased neurogenesis and spinogenesis might be associated, at least in part, with deficits in memory formation in *Stat4A* mice.

We investigated the specific role of stathmin in memory processing and found that stathmin function is required for both the acquisition and retrieval of contextual fear memory. In addition, *Stat4A* mice displayed a deficit in spatial memory acquisition. It is interesting to note that adult-born DCX-positive immature neurons in the DG are required for the successful acquisition of spatial learning as well as reversal learning (Vukovic et al., 2013). Importantly, we found that endogenous stathmin is enriched in DCX-positive cells and that, in *Stat4A* mice, the transgene is highly expressed in DCX-positive neurons. Together, our data suggest that, in DCX-positive immature neurons, stathmin might regulate the acquisition of memories. Our data also suggest the involvement of stathmin in memory recall. Although a recent report indicated that DCX-positive neurons are not necessary for the retrieval of stored long-term memory (Vukovic et al., 2013), other work has suggested that adult-born neurons are required for memory recall (Arruda-Carvalho et al., 2011; Gu et al., 2012). Thus, stathmin activity in DCX-positive neurons might be im-

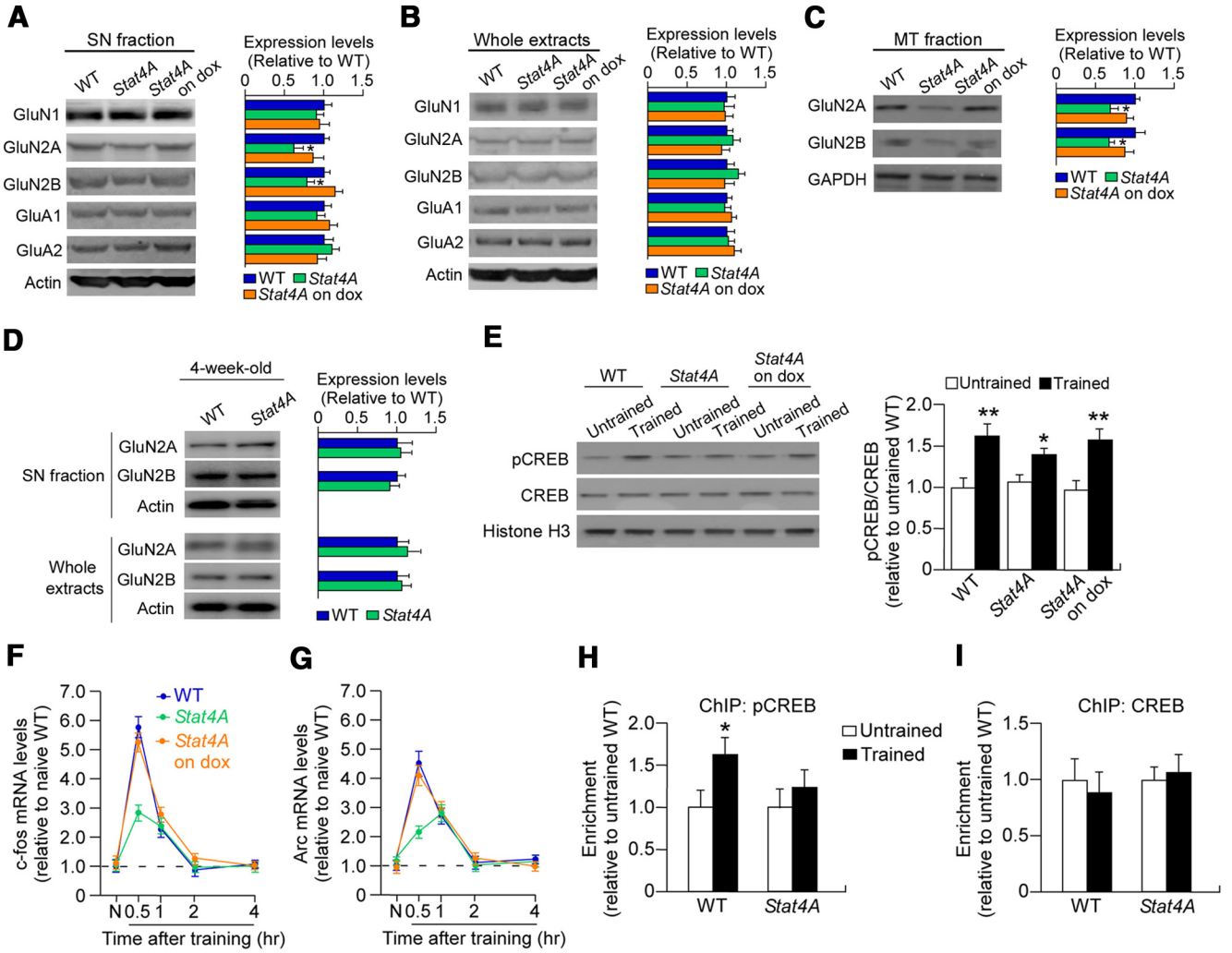

Figure 10. Decreased synaptic NMDAR and CREB-mediated gene transcription in *Stat4A* mice. ***A–C***, Western blotting reveals the levels of GluN1, GluN2A, GluN2B, GluA1, and GluA2 in the synaptosomal (SN) fractions (***A***), whole-cell extracts (***B***), and microtubule (MT) fractions (***C***) from the DG of naive WT and *Stat4A* mice fed with or without dox. The results reveal reduced GluN2A and GluN2B levels in SN and MT fractions in *Stat4A* mice. $n = 6$ for each group. $^*p < 0.05$ versus WT mice. ***D***, Western blotting reveals the levels of GluN2A and GluN2B in the SN fractions and whole-cell extracts from the DG of juvenile (4-week-old) WT and *Stat4A* mice. ***E***, Western blotting reveals that *Stat4A* mice that were not administered dox exhibit weak induction of pCREB in the DG after contextual fear conditioning, compared with WT or *Stat4A* mice administered dox (on dox). $n = 6$ for each group. $^*p < 0.05$ versus naive (untrained) mice in the corresponding genotype. $^{**}p < 0.01$ versus naive (untrained) mice in the corresponding genotype. ***F***, ***G***, Real-time PCR reveals reduced mRNA induction for *c-fos* (***F***) and *Arc* (***G***) in the DG in *Stat4A* mice. $n = 6$ for each group. $^*p < 0.05$ versus WT mice. ***H***, ***I***, ChIP assay showing the recruitment of pCREB (***H***) or total CREB (***I***) to the *c-fos* promoter. $^*p < 0.05$ versus untrained mice. Data are mean ± SEM.

portant for memory acquisition, whereas its role in recall remains unclear.

The present work on the intracellular transport of the GluN2A and GluN2B subunits of the NMDAR in basal (naive) conditions adds to the earlier finding that the stathmin-mediated enhancement of microtubule stability following learning controls KIF5-induced dendritic transport of the GluA2 subunit of the AMPA receptor (Uchida et al., 2014). *Stat4A* mice exhibited reduced synaptosomal GluA2 and impaired KIF5-GluA2 interaction following contextual fear conditioning. By contrast, GluA2 levels were normal in the naive state in *Stat4A* mice. Thus, the dendritic transport of GluA2 along microtubules appears to be regulated by stathmin in a learning (activity)-dependent manner. Conversely, synaptosomal GluN2A and GluN2B levels are reduced in naive *Stat4A* mice, suggesting that stathmin also plays an important role in constitutive dendritic transport. These findings are consistent with earlier work revealing that the microtubule-mediated constitutive synaptic localization of GluN2A and GluN2B is regulated by KIF17 and that KIF17-dependent synaptic transport of NMDARs is important for CREB activation and memory formation (Yin et al., 2011). Therefore, stathmin regulates the dendritic transport of postsynaptically localized glutamatergic receptors in both basal (NMDAR) and learning-dependent (AMPAR) states.

We found that learning-induced CREB-mediated gene transcription is downregulated in *Stat4A* mice. The deficits in NMDAR-dependent and CREB-mediated gene transcription, adult neurogenesis, spinogenesis, and memory in *Stat4A* mice are in agreement with the known roles of CREB in these processes (Murphy and Segal, 1997; Silva et al., 1998; Kida et al., 2002; Nakagawa et al., 2002; Jagasia et al., 2009; Kandel, 2012). Our data showing the importance of the stathmin-CREB link in memory processes together with findings regarding the role of CREB-stathmin interactions in the preservation of interphase microtubules in response to hyperosmotic stress (Yip et al., 2014) suggest that this molecular signaling pathway may work as a general mechanism across different biological processes.

Despite the fact that *Stat4A* transgene is expressed in only 13% of NeuN-positive mature neurons in mutant mice, we found

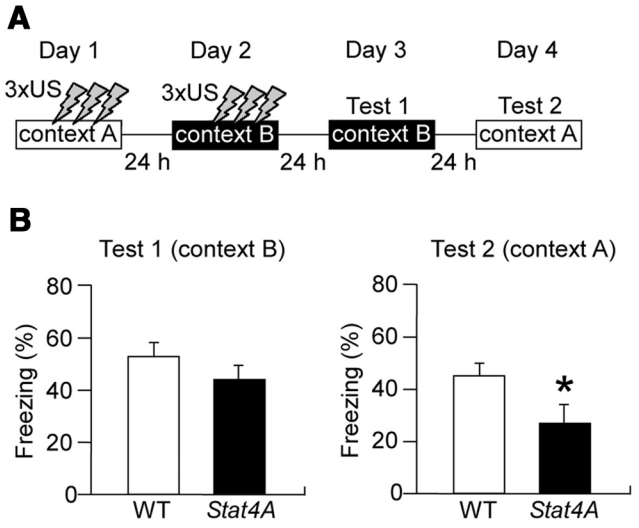

Figure 11. Normal NMDAR-independent memory in *Stat4A* mice. ***A***, Experimental design. Mice were trained in context A on day 1 and in context B on day 2. Subsequently, they were tested for freezing in contexts B (Test 1) and A (Test 2) on days 3 and 4, respectively. ***B***, *Stat4A* mice display normal fear memory in context B but reduced fear memory in context A. $n = 11–13$ for each group. $^*p < 0.05$. Data are mean ± SEM.

significant differences in spinogenesis, synaptic localization of NMDAR, and learning-dependent c-fos mRNA induction. A previous report also has shown that gene manipulation in adult hippocampal stem and progenitor cells leads to altered neurogenesis as well as reduced spine density, long-term potentiation, c-fos expression in mature neurons, and memory formation (Farioli-Vecchioli et al., 2008). The newly generated DG granule neurons seem to involve targeting to preexisting synaptic partners, which suggests a role for circuit activity in the integration of adult-born DG granule neurons (Deng et al., 2010). Thus, stathmin activation in the DCX-positive neurons may affect, at least in part, an integration of new neurons into preexisting neuronal population within the DG, which then modulate memory circuits.

Although transgenic stathmin is expressed in the lateral amygdala, we did not observe any differences in amygdala-dependent memory and the morphology of the dendritic spines of principal neurons in the lateral amygdala in *Stat4* mice. It is possible that microtubules are hyperstable in the amygdala due to the strong endogenous expression of phosphorylated stathmin, which blocks the effects of mutant *Stat4A*. In addition, juvenile *Stat4A* mice did not exhibit any abnormalities in maturation of DCX-positive cells or in the spine density of DG granule neurons, suggesting that *Stat4A* overexpression does not affect these processes during development. Supporting this notion, *Stat4A* mice and stathmin knock-out mice display normal hippocampus morphology (Shumyatsky et al., 2005; Boekhoorn et al., 2014; Uchida et al., 2014). Stathmin family proteins include stathmin (stathmin 1), stathmin 2 (SCG10), stathmin 3 (SCLIP), and stathmin 4 (RB3). Interestingly, stathmin is the only protein expressed during postnatal development and adulthood, whereas the expression of stathmins 2–4 is strong during development but not in adulthood (Boekhoorn et al., 2014), suggesting that stathmin 2–4 could compensate for the loss of microtubule stability induced by *Stat4A* overexpression during development.

In conclusion, our data identify stathmin as an important molecule in the regulation of adult neurogenesis and spinogenesis in the DG. We further demonstrate a causal relationship between stathmin-mediated neuronal maturation and hippocampus-dependent learning and memory. Our study also provides evidence for a role of stathmin-mediated microtubule dynamics in experience-dependent CREB-mediated gene transcription. These findings demonstrate the role of stathmin-mediated microtubule dynamics in neurogenesis-dependent memory formation through modulation of the NMDAR-CREB signaling pathway.

References

Aimone JB, Deng W, Gage FH (2011) Resolving new memories: a critical look at the dentate gyrus, adult neurogenesis, and pattern separation. Neuron 70:589–596. CrossRef Medline

Amat JA, Fields KL, Schubart UK (1991) Distribution of phosphoprotein p19 in rat brain during ontogeny: stage-specific expression in neurons and glia. Brain Res Dev Brain Res 60:205–218. CrossRef Medline

Arruda-Carvalho M, Sakaguchi M, Akers KG, Josselyn SA, Frankland PW (2011) Posttraining ablation of adult-generated neurons degrades previously acquired memories. J Neurosci 31:15113–15127. CrossRef Medline

Bach ME, Hawkins RD, Osman M, Kandel ER, Mayford M (1995) Impairment of spatial but not contextual memory in CaMKII mutant mice with a selective loss of hippocampal LTP in the range of the theta frequency. Cell 81:905–915. CrossRef Medline

Belmont LD, Mitchison TJ (1996) Identification of a protein that interacts with tubulin dimers and increases the catastrophe rate of microtubules. Cell 84:623–631. CrossRef Medline

Beretta L, Dobránsky T, Sobel A (1993) Multiple phosphorylation of stathmin: identification of four sites phosphorylated in intact cells and in vitro by cyclic AMP-dependent protein kinase and p34cdc2. J Biol Chem 268:20076–20084. Medline

Boekhoorn K, van Dis V, Goedknegt E, Sobel A, Lucassen PJ, Hoogenraad CC (2014) The microtubule destabilizing protein stathmin controls the transition from dividing neuronal precursors to postmitotic neurons during adult hippocampal neurogenesis. Dev Neurobiol 74:1226–1242. CrossRef Medline

Bourtchuladze R, Frenguelli B, Blendy J, Cioffi D, Schutz G, Silva AJ (1994) Deficient long-term memory in mice with a targeted mutation of the cAMP-responsive element-binding protein. Cell 79:59–68. CrossRef Medline

Calandreau L, Desmedt A, Decorte L, Jaffard R (2005) A different recruitment of the lateral and basolateral amygdala promotes contextual or elemental conditioned association in Pavlovian fear conditioning. Learn Mem 12:383–388. CrossRef Medline

Clelland CD, Choi M, Romberg C, Clemenson GD Jr, Fragniere A, Tyers P, Jessberger S, Saksida LM, Barker RA, Gage FH, Bussey TJ (2009) A functional role for adult hippocampal neurogenesis in spatial pattern separation. Science 325:210–213. CrossRef Medline

Clement JP, Aceti M, Creson TK, Ozkan ED, Shi Y, Reish NJ, Almonte AG, Miller BH, Wiltgen BJ, Miller CA, Xu X, Rumbaugh G (2012) Pathogenic SYNGAP1 mutations impair cognitive development by disrupting maturation of dendritic spine synapses. Cell 151:709–723. CrossRef Medline

Curmi PA, Gavet O, Charbaut E, Ozon S, Lachkar-Colmerauer S, Manceau V, Siavoshian S, Maucuer A, Sobel A (1999) Stathmin and its phosphoprotein family: general properties, biochemical and functional interaction with tubulin. Cell Struct Funct 24:345–357. CrossRef Medline

David DJ, Samuels BA, Rainer Q, Wang JW, Marsteller D, Mendez I, Drew M, Craig DA, Guiard BP, Guilloux JP, Artymyshyn RP, Gardier AM, Gerald C, Antonijevic IA, Leonardo ED, Hen R (2009) Neurogenesis-dependent and -independent effects of fluoxetine in an animal model of anxiety/depression. Neuron 62:479–493. CrossRef Medline

Deng W, Saxe MD, Gallina IS, Gage FH (2009) Adult-born hippocampal dentate granule cells undergoing maturation modulate learning and memory in the brain. J Neurosci 29:13532–13542. CrossRef Medline

Deng W, Aimone JB, Gage FH (2010) New neurons and new memories: how does adult hippocampal neurogenesis affect learning and memory? Nat Rev Neurosci 11:339–350. CrossRef Medline

Denis-Donini S, Dellarole A, Crociara P, Francese MT, Bortolotto V, Quadrato G, Canonico PL, Orsetti M, Ghi P, Memo M, Bonini SA, Ferrari-Toninelli G, Grilli M (2008) Impaired adult neurogenesis associated with short-term memory defects in NF-kappaB p50-deficient mice. J Neurosci 28:3911–3919. CrossRef Medline

Desmedt A, Garcia R, Jaffard R (1998) Differential modulation of changes in hippocampal-septal synaptic excitability by the amygdala as a function of either elemental or contextual fear conditioning in mice. J Neurosci 18:480–487. Medline

Desmedt A, Hazvi S, Dudai Y (2003) Differential pattern of cAMP response element-binding protein activation in the rat brain after conditioned aversion as a function of the associative process engaged: taste versus context association. J Neurosci 23:6102–6110. Medline

Di Paolo G, Antonsson B, Kassel D, Riederer BM, Grenningloh G (1997) Phosphorylation regulates the microtubule-destabilizing activity of stathmin and its interaction with tubulin. FEBS Lett 416:149–152. CrossRef Medline

Drew LJ, Fusi S, Hen R (2013) Adult neurogenesis in the mammalian hippocampus: why the dentate gyrus? Learn Mem 20:710–729. CrossRef Medline

Farioli-Vecchioli S, Saraulli D, Costanzi M, Pacioni S, Cinà I, Aceti M, Micheli L, Bacci A, Cestari V, Tirone F (2008) The timing of differentiation of adult hippocampal neurons is crucial for spatial memory. PLoS Biol 6:e246. CrossRef Medline

Frankland PW (2013) Neurogenic evangelism: comment on Urbach et al. (2013). Behav Neurosci 127:126–129. CrossRef Medline

Fuster-Matanzo A, Llorens-Martín M, Jurado-Arjona J, Avila J, Hernandez F (2012) Tau protein and adult hippocampal neurogenesis. Front Neurosci 6:104. CrossRef Medline

Gu Y, Arruda-Carvalho M, Wang J, Janoschka SR, Josselyn SA, Frankland PW, Ge S (2012) Optical controlling reveals time-dependent roles for adult-born dentate granule cells. Nat Neurosci 15:1700–1706. CrossRef Medline

Guo W, Allan AM, Zong R, Zhang L, Johnson EB, Schaller EG, Murthy AC, Goggin SL, Eisch AJ, Oostra BA, Nelson DL, Jin P, Zhao X (2011) Ablation of Fmrp in adult neural stem cells disrupts hippocampus-dependent learning. Nat Med 17:559–565. CrossRef Medline

Hagihara H, Toyama K, Yamasaki N, Miyakawa T (2009) Dissection of hippocampal dentate gyrus from adult mouse. J Vis Exp 33:pii1543. CrossRef Medline

Hamilton AM, Oh WC, Vega-Ramirez H, Stein IS, Hell JW, Patrick GN, Zito K (2012) Activity-dependent growth of new dendritic spines is regulated by the proteasome. Neuron 74:1023–1030. CrossRef Medline

Hirokawa N, Niwa S, Tanaka Y (2010) Molecular motors in neurons: transport mechanisms and roles in brain function, development, and disease. Neuron 68:610–638. CrossRef Medline

Imayoshi I, Sakamoto M, Ohtsuka T, Takao K, Miyakawa T, Yamaguchi M, Mori K, Ikeda T, Itohara S, Kageyama R (2008) Roles of continuous neurogenesis in the structural and functional integrity of the adult forebrain. Nat Neurosci 11:1153–1161. CrossRef Medline

Impey S, Mark M, Villacres EC, Poser S, Chavkin C, Storm DR (1996) Induction of CRE-mediated gene expression by stimuli that generate long-lasting LTP in area CA1 of the hippocampus. Neuron 16:973–982. CrossRef Medline

Jagasia R, Steib K, Englberger E, Herold S, Faus-Kessler T, Saxe M, Gage FH, Song H, Lie DC (2009) GABA-cAMP response element-binding protein signaling regulates maturation and survival of newly generated neurons in the adult hippocampus. J Neurosci 29:7966–7977. CrossRef Medline

Jaglin XH, Chelly J (2009) Tubulin-related cortical dysgeneses: microtubule dysfunction underlying neuronal migration defects. Trends Genet 25:555–566. CrossRef Medline

Jaworski J, Kapitein LC, Gouveia SM, Dortland BR, Wulf PS, Grigoriev I, Camera P, Spangler SA, Di Stefano P, Demmers J, Krugers H, Defilippi P, Akhmanova A, Hoogenraad CC (2009) Dynamic microtubules regulate dendritic spine morphology and synaptic plasticity. Neuron 61:85–100. CrossRef Medline

Jin K, Mao XO, Cottrell B, Schilling B, Xie L, Row RH, Sun Y, Peel A, Childs J, Gendeh G, Gibson BW, Greenberg DA (2004) Proteomic and immunochemical characterization of a role for stathmin in adult neurogenesis. FASEB J 18:287–299. CrossRef Medline

Kandel ER (2012) The molecular biology of memory: cAMP, PKA, CRE, CREB-1, CREB-2, and CPEB. Mol Brain 5:14. CrossRef Medline

Kapitein LC, Yau KW, Hoogenraad CC (2010) Microtubule dynamics in dendritic spines. Methods Cell Biol 97:111–132. CrossRef Medline

Kheirbek MA, Tannenholz L, Hen R (2012) NR2B-dependent plasticity of adult-born granule cells is necessary for context discrimination. J Neurosci 32:8696–8702. CrossRef Medline

Kida S, Josselyn SA, Peña de Ortiz S, Kogan JH, Chevere I, Masushige S, Silva AJ (2002) CREB required for the stability of new and reactivated fear memories. Nat Neurosci 5:348–355. CrossRef Medline

Kim JJ, Fanselow MS (1992) Modality-specific retrograde amnesia of fear. Science 256:675–677. CrossRef Medline

Küntziger T, Gavet O, Sobel A, Bornens M (2001) Differential effect of two stathmin/Op18 phosphorylation mutants on *Xenopus* embryo development. J Biol Chem 276:22979–22984. CrossRef Medline

Larsson N, Marklund U, Gradin HM, Brattsand G, Gullberg M (1997) Control of microtubule dynamics by oncoprotein 18: dissection of the regulatory role of multisite phosphorylation during mitosis. Mol Cell Biol 17:5530–5539. CrossRef Medline

Lau CG, Zukin RS (2007) NMDA receptor trafficking in synaptic plasticity and neuropsychiatric disorders. Nat Rev Neurosci 8:413–426. CrossRef Medline

Lee YS, Silva AJ (2009) The molecular and cellular biology of enhanced cognition. Nat Rev Neurosci 10:126–140. CrossRef Medline

le Gouvello S, Manceau V, Sobel A (1998) Serine 16 of stathmin as a cytosolic target for Ca^{2+}/calmodulin-dependent kinase II after CD2 triggering of human T lymphocytes. J Immunol 161:1113–1122. Medline

Leutgeb JK, Leutgeb S, Moser MB, Moser EI (2007) Pattern separation in the dentate gyrus and CA3 of the hippocampus. Science 315:961–966. CrossRef Medline

Lonze BE, Ginty DD (2002) Function and regulation of CREB family transcription factors in the nervous system. Neuron 35:605–623. CrossRef Medline

Marklund U, Larsson N, Brattsand G, Osterman O, Chatila TA, Gullberg M (1994) Serine 16 of oncoprotein 18 is a major cytosolic target for the Ca^{2+}/calmodulin-dependent kinase-Gr. Eur J Biochem 225:53–60. CrossRef Medline

Martel G, Hevi C, Friebely O, Baybutt T, Shumyatsky GP (2010) Zinc transporter 3 is involved in learned fear and extinction, but not in innate fear. Learn Mem 17:582–590. CrossRef Medline

Martel G, Hevi C, Kane-Goldsmith N, Shumyatsky GP (2011) Zinc transporter ZnT3 is involved in memory dependent on the hippocampus and perirhinal cortex. Behav Brain Res 223:233–238. CrossRef Medline

McHugh TJ, Jones MW, Quinn JJ, Balthasar N, Coppari R, Elmquist JK, Lowell BB, Fanselow MS, Wilson MA, Tonegawa S (2007) Dentate gyrus NMDA receptors mediate rapid pattern separation in the hippocampal network. Science 317:94–99. CrossRef Medline

Meshi D, Drew MR, Saxe M, Ansorge MS, David D, Santarelli L, Malapani C, Moore H, Hen R (2006) Hippocampal neurogenesis is not required for behavioral effects of environmental enrichment. Nat Neurosci 9:729–731. CrossRef Medline

Morris RG, Garrud P, Rawlins JN, O'Keefe J (1982) Place navigation impaired in rats with hippocampal lesions. Nature 297:681–683. CrossRef Medline

Murphy DD, Segal M (1997) Morphological plasticity of dendritic spines in central neurons is mediated by activation of cAMP response element binding protein. Proc Natl Acad Sci U S A 94:1482–1487. CrossRef Medline

Nacher J, McEwen BS (2006) The role of N-methyl-D-asparate receptors in neurogenesis. Hippocampus 16:267–270. CrossRef Medline

Nakagawa S, Kim JE, Lee R, Malberg JE, Chen J, Steffen C, Zhang YJ, Nestler EJ, Duman RS (2002) Regulation of neurogenesis in adult mouse hippocampus by cAMP and the cAMP response element-binding protein. J Neurosci 22:3673–3682. Medline

Nakashiba T, Cushman JD, Pelkey KA, Renaudineau S, Buhl DL, McHugh TJ, Rodriguez Barrera V, Chittajallu R, Iwamoto KS, McBain CJ, Fanselow MS, Tonegawa S (2012) Young dentate granule cells mediate pattern separation, whereas old granule cells facilitate pattern completion. Cell 149:188–201. CrossRef Medline

Ohkawa N, Fujitani K, Tokunaga E, Furuya S, Inokuchi K (2007a) The microtubule destabilizer stathmin mediates the development of dendritic arbors in neuronal cells. J Cell Sci 120:1447–1456. CrossRef Medline

Ohkawa N, Hashimoto K, Hino T, Migishima R, Yokoyama M, Kano M, Inokuchi K (2007b) Motor discoordination of transgenic mice overexpressing a microtubule destabilizer, stathmin, specifically in Purkinje cells. Neurosci Res 59:93–100. CrossRef Medline

Pan YW, Chan GC, Kuo CT, Storm DR, Xia Z (2012) Inhibition of adult neurogenesis by inducible and targeted deletion of ERK5 mitogen-activated protein kinase specifically in adult neurogenic regions impairs

contextual fear extinction and remote fear memory. J Neurosci 32: 6444–6455. CrossRef Medline

Paxinos G, Franklin K (2001) The mouse brain in stereotaxic coordinates, Ed 2. San Diego: Academic.

Rampon C, Tang YP, Goodhouse J, Shimizu E, Kyin M, Tsien JZ (2000) Enrichment induces structural changes and recovery from nonspatial memory deficits in CA1 NMDAR1-knockout mice. Nat Neurosci 3:238–244. CrossRef Medline

Sahay A, Scobie KN, Hill AS, O'Carroll CM, Kheirbek MA, Burghardt NS, Fenton AA, Dranovsky A, Hen R (2011) Increasing adult hippocampal neurogenesis is sufficient to improve pattern separation. Nature 472: 466–470. CrossRef Medline

Saxe MD, Battaglia F, Wang JW, Malleret G, David DJ, Monckton JE, Garcia AD, Sofroniew MV, Kandel ER, Santarelli L, Hen R, Drew MR (2006) Ablation of hippocampal neurogenesis impairs contextual fear conditioning and synaptic plasticity in the dentate gyrus. Proc Natl Acad Sci U S A 103:17501–17506. CrossRef Medline

Shumyatsky GP, Tsvetkov E, Malleret G, Vronskaya S, Hatton M, Hampton L, Battey JF, Dulac C, Kandel ER, Bolshakov VY (2002) Identification of a signaling network in lateral nucleus of amygdala important for inhibiting memory specifically related to learned fear. Cell 111:905–918. CrossRef Medline

Shumyatsky GP, Malleret G, Shin RM, Takizawa S, Tully K, Tsvetkov E, Zakharenko SS, Joseph J, Vronskaya S, Yin D, Schubart UK, Kandel ER, Bolshakov VY (2005) stathmin, a gene enriched in the amygdala, controls both learned and innate fear. Cell 123:697–709. CrossRef Medline

Silva AJ, Kogan JH, Frankland PW, Kida S (1998) CREB and memory. Annu Rev Neurosci 21:127–148. CrossRef Medline

Sobel A (1991) Stathmin: a relay phosphoprotein for multiple signal transduction? Trends Biochem Sci 16:301–305. CrossRef Medline

Tang YP, Shimizu E, Dube GR, Rampon C, Kerchner GA, Zhuo M, Liu G, Tsien JZ (1999) Genetic enhancement of learning and memory in mice. Nature 401:63–69. CrossRef Medline

Tashiro A, Sandler VM, Toni N, Zhao C, Gage FH (2006) NMDA-receptor-mediated, cell-specific integration of new neurons in adult dentate gyrus. Nature 442:929–933. CrossRef Medline

Trifilieff P, Herry C, Vanhoutte P, Caboche J, Desmedt A, Riedel G, Mons N, Micheau J (2006) Foreground contextual fear memory consolidation requires two independent phases of hippocampal ERK/CREB activation. Learn Mem 13:349–358. CrossRef Medline

Tsien JZ, Huerta PT, Tonegawa S (1996) The essential role of hippocampal CA1 NMDA receptor-dependent synaptic plasticity in spatial memory. Cell 87:1327–1338. CrossRef Medline

Uchida S, Shumyatsky GP (2015) Deceivingly dynamic: learning-dependent changes in stathmin and microtubules. Neurobiol Learn Mem 124:52–61. CrossRef Medline

Uchida S, Hara K, Kobayashi A, Funato H, Hobara T, Otsuki K, Yamagata H, McEwen BS, Watanabe Y (2010) Early life stress enhances behavioral vulnerability to stress through the activation of REST4-mediated gene transcription in the medial prefrontal cortex of rodents. J Neurosci 30: 15007–15018. CrossRef Medline

Uchida S, Hara K, Kobayashi A, Otsuki K, Yamagata H, Hobara T, Suzuki T, Miyata N, Watanabe Y (2011a) Epigenetic status of Gdnf in the ventral striatum determines susceptibility and adaptation to daily stressful events. Neuron 69:359–372. CrossRef Medline

Uchida S, Hara K, Kobayashi A, Fujimoto M, Otsuki K, Yamagata H, Hobara T, Abe N, Higuchi F, Shibata T, Hasegawa S, Kida S, Nakai A, Watanabe Y (2011b) Impaired hippocampal spinogenesis and neurogenesis and altered affective behavior in mice lacking heat shock factor 1. Proc Natl Acad Sci U S A 108:1681–1686. CrossRef Medline

Uchida S, Martel G, Pavlowsky A, Takizawa S, Hevi C, Watanabe Y, Kandel ER, Alarcon JM, Shumyatsky GP (2014) Learning-induced and stathmin-dependent changes in microtubule stability are critical for memory and disrupted in ageing. Nat Commun 5:4389. CrossRef Medline

Vukovic J, Borlikova GG, Ruitenberg MJ, Robinson GJ, Sullivan RK, Walker TL, Bartlett PF (2013) Immature doublecortin-positive hippocampal neurons are important for learning but not for remembering. J Neurosci 33:6603–6613. CrossRef Medline

Wang JW, David DJ, Monckton JE, Battaglia F, Hen R (2008) Chronic fluoxetine stimulates maturation and synaptic plasticity of adult-born hippocampal granule cells. J Neurosci 28:1374–1384. CrossRef Medline

West AE, Griffith EC, Greenberg ME (2002) Regulation of transcription factors by neuronal activity. Nat Rev Neurosci 3:921–931. CrossRef Medline

Wiltgen BJ, Royle GA, Gray EE, Abdipranoto A, Thangthaeng N, Jacobs N, Saab F, Tonegawa S, Heinemann SF, O'Dell TJ, Fanselow MS, Vissel B (2010) A role for calcium-permeable AMPA receptors in synaptic plasticity and learning. PLoS One 5:piie12818. CrossRef Medline

Yin X, Takei Y, Kido MA, Hirokawa N (2011) Molecular motor KIF17 is fundamental for memory and learning via differential support of synaptic NR2A/2B levels. Neuron 70:310–325. CrossRef Medline

Yip YY, Yeap YY, Bogoyevitch MA, Ng DC (2014) cAMP-dependent protein kinase and c-Jun N-terminal kinase mediate stathmin phosphorylation for the maintenance of interphase microtubules during osmotic stress. J Biol Chem 289:2157–2169. CrossRef Medline

Yuen EY, Jiang Q, Feng J, Yan Z (2005) Microtubule regulation of N-methyl-D-aspartate receptor channels in neurons. J Biol Chem 280: 29420–29427. CrossRef Medline

Zhang CL, Zou Y, He W, Gage FH, Evans RM (2008a) A role for adult TLX-positive neural stem cells in learning and behaviour. Nature 451: 1004–1007. CrossRef Medline

Zhang M, Moon C, Chan GC, Yang L, Zheng F, Conti AC, Muglia L, Muglia LJ, Storm DR, Wang H (2008b) Ca-stimulated type 8 adenylyl cyclase is required for rapid acquisition of novel spatial information and for working/episodic-like memory. J Neurosci 28:4736–4744. CrossRef Medline

Zhu JJ, Qin Y, Zhao M, Van Aelst L, Malinow R (2002) Ras and Rap control AMPA receptor trafficking during synaptic plasticity. Cell 110:443–455. CrossRef Medline